THE OBSERVATION OF ULTRASONIC VELOCITIES AND ATTENUATION DURING PORE PRESSURE INDUCED FRACTURE

by

Thomas Edward Hess

B.S. Massachusetts Institute of Technology (1981)

SUBMITTED TO THE DEPARTMENT OF EARTH, ATMOSPHERIC AND PLANETARY SCIENCES IN PARTIAL FULFILLMENT OF THE REQUIREMENTS FOR THE DEGREE OF

MASTER OF SCIENCE IN EARTH, ATMOSPHERIC AND PLANETARY SCIENCES

at the

MASSACHUSETTS INSTITUTE OF TECHNOLOGY

October 1983

Signature of Author _____
Department of Earth, Atmospheric and Planetary Sciences
October 11, 1983

Certified by _____
Michael P. Cleary and M. Nafi Toksoz
Thesis Supervisors

Accepted by _____
Theodore R. Madden
Chairman, Departmental Committee on Graduate Students

The Observation of
Ultrasonic Velocities
and Attenuation During Pore Pressure
Induced Fracture

by

Thomas Edward Hess

Submitted to the Department of Earth, Atmospheric and Planetary Sciences on October 11, 1983 in partial fulfillment of the requirements for the degree of Master of Science in Earth, Atmospheric and Planetary Sciences.

Abstract

The creation of an excessively high pore pressure causes damage to the microstructure of a porous material by causing the matrix to crack from the stress of the fluid in the pore space. The cracks affect on dynamically measured velocities, attenuation and strain was limited by the length of time that the excessive pressure was present within the pore spaces. The fluid pressure was allowed to decrease with time as diffussive flow occurred. Saturation was maintained by preventing fluid from flowing from the sample with a base value of confining pressure and pore pressure.

Microcracks in the fractured material were different than the ones present in the virgin samples. Aside from an increase in the apparent number of cracks in the fractured material the aspect ratio decreased significantly as the lengths of the cracks dramatically increased.

Velocities were observed to increase after pore pressure was allowed to be at it's highest state and decay to a steady-state value. Attenuation of the wave amplitudes was observed to change, P wave amplitude increased with time and the difference in S wave amplitude was neglectable.

Observation of dynamic fracture behavior on the microstructural level from velocity shifts, strain data, and relative attenuation correspond to the scanning

electron microscope observations that microcracks are formed due to the creation of effective tensile stresses by the excessive pore pressure in the experimental proceedure. In addition, data points towards the creation of two distinct types of damage to the microstructure: one having a permanent nature and the other dynamically changing as the internal pore pressure is relieved with time. As the number of cycles increases, the resulting transient damage decreases, but the corresponding permanent damage reaches a constant level as indicated by the resulting attenuation and velocity changes.

Thesis Supervisor: M. Nafi Toksoz
Title: Professor of Geophysics

Michael P. Cleary
Associate Professor
Mechanical Engineering

Table of Contents

List of Figures

Acknowledgements

I wish to thank, first Professor Micheal P. Cleary for his untiring efforts to instill vigilance in all my work. Professor Cleary's efforts to overcome the immense difficulties involved with getting this project off the ground are deeply appreciated. As well the many members of the Resource Extraction Lab and the department of Mechanical Engineering were extremely helpful. The Mining and Mineral Resources Research Institute directed by Professor John Elliot provided the much needed funding that made this possible. I also wish to thank Professor Nafi Toksoz for providing good advice on the use and validity of my data. Karl Coyner provided much advice on the construction and design of the system.

I owe a great deal to my fellow student, Aaron Heintz, who was familar with many details that I would have had much difficulty correcting without him. Through his "Fear and Loathing" methods we spent many long hours torturing the equipment for data. I wish to thank Larry Hsu, Aaron's understudy, who will probably never have regular sleep habits again.

I found Robert "Benjie" Ambrogi to not only draw good figures, but to have been a source of encouragement in some of the most frustrating times.

Without Mike Davis much of the interacting programs for data manipulation and analysis never would have been done on time. His penchant for detail and his untiring efforts have contributed immensely to my work.

My two coworkers, Phil Soo and Suki Vogeler were much help in preparing samples and analyzing the static properties to insure homogeneous samples. As well, Suki makes the worst coffee in the world.

Life at the Resource Extraction Lab would have suffered without the good humor and help provided by Susan Bimbo. As well, Joe Parse and Richard Keck provided Susan with much material for general mutual humor.

My deepest gratitude goes out to my housemates and friends of several years whom provided a family in Cambridge: Terry Crowley, Ann Welch, Mark Dudley, Kristin Brockelman(now Mrs. Dudley), and Barry Landau. Last but not least I am indebted to Dave Bower for his copy editing of this manuscript and for his boathouse which restored my sanity in many cases.

For Mom

1 Introduction

The effect of pore fluids upon the physical state of rock materials is not well understood. The fluids can play many complex and interactive roles in the modification of the properties of rock. Pore spaces and their geometry also play a large role in their effect on the materials physical properties.

In this study the pore fluid's affect on the material matrix is observed through the use of ultrasonic wave propagation techniques, dynamic strain measurements and direct electron microscope observations. The pore fluid pressure is allowed to exceed the confining stresses, thereby moving the effective stress state of the matrix into the tensile region. This overpressuring of the pore spaces models several conditions that can significantly affect much of the data collected by *in situ* methods where the pore pressure has been suddenly altered by a difference at least equal to those in this study. In a wellbore the fluids or mud that is used in the hole will affect the areas adjacent to the bore that experience the excess fluid pressure. The pore pressure may damage the microstructure by fracturing the solid matrix along prefered flaws or crack tips. An increase in the number and length of cracks within the fractured specimen is seen by scanning electron microscope observations as well as by the shift in velocities and wave amplitudes.

Rocks suddenly brought to the surface have high pore pressure. These cores are damaged by the same physical process that is used in this experiment. Cracks that are present in samples used to model *in situ* conditions may be there as a result of the extraction process, and the results may deviate further from true *in situ* values than previously suspected.

Induced pore pressure fracture, or pore pressure induced cracking (PPIC),

is a process in which many small fractures are created or extended in a porous material by saturating the pore space with pressurized fluid and then reducing the external confining stress, thus increasing the effective stress. Using wave propagation techniques it is possible to understand some of the parameters controling the fracture event. The results should be useful in predicting changes (e.g. of permeability and strength) in underground rock when it is subjected to similar conditions (e.g. for enhanced drilling, fracturing or cavity formation.)

Thus far, uniform and homogeneous mortar(cement) specimens have been created for the purposes of this experiment. The composition of the mortar was determined, based on the extent to which fracture occured. A ratio of 1:1:0.8 cement:sand:water was chosen because it exhibited the most pronounced effects of pore fluid fracture.

Preliminary tests were done on the specimens to create pore fluid fracture using different fluids, including air, and various stress drops. The mechanical effect of pore fluid fracture was indicated by a drop in tensile strength (obtained with Brazilian diametral compression test.)

Initially during the tests, the pressure inside is p_p and the pressure outside the rock is p_o the effective stress is therefore zero at the edges of the rock and p_p-p_o in the center of the rock. When the rock is saturated with the externally pressurized fluid, the effective stress everywhere is zero. When the pressure is reduced outside the rock, the effective stress again quickly goes towards zero, acheiving a steady state of p_∞ near the surface of the rock but the effective stress inside the rock is p_∞-p_p where p_p is the pore pressure reducing with time as diffusive flow occurs This final state of stress is responsible for the microfractures observed in the samples.

The relationships between confining stress- pore fluid pressure and material response are also dramatized. The understanding of these relations will help predict the reactions of underground rocks to sudden drops of pressure that occur, for example, when they are being drilled or fractured. Eventually, with the rock's characteristics, the pore fluid conditions and the pressure drop, one may expect to be able to predict how much the structure and dynamic response of the rock will change.

Chapter one describes some of the background necessary for an understanding of induced pore pressure fracture and the use of wave propagation methods. The examination of the wave properties constrains the dynamic changes within the sample during the fracture event. All the elastic moduli as well as the ultrasonic wavelet itself contribute to the understanding of how the cracks are behaving. The equations in the first chapter will describe the loss of pore pressure with time in our cylindrical samples. This also describes the period of time during which the velocities and attenuation shift .

Chapter two describes the techniques involved in measuring the velocity and attenuation of the samples. The wave propagation methods are familar techniques and no attempt is made to describe them in great detail. An analysis of the errors present within the measurements is also included to constrain the validity of the data.

The data is presented and interpreted in Chapter Three. The changes in velocity attenuation and strain data are presented with respect to time. The phenomena is interpreted with respect to the observations on the electron microscope and static strength tests included in the appendix.

Chapter 1
Experimental Parameters

1.1 Fluid Parameters

Examination of the effects of induced pore pressure fracture can be approximated by the equations of fluid transport. The situation used to fracture the microstructure requires that the pore pressure exceeds the tensile strength of the material. No attempt is made to completely solve the problem explicitly, but rather a qualitative picture is presented here.

The primary parameter of interest in fluid transport phenomena is the material's fluid permeability as defined by Darcy's equations:

$$q_i = (k_{ij}/\mu)\ (\partial P/\partial x_j) \tag{1.1}$$

where μ is the viscosity of the fluid, P is pressure, q is the flow rate, and k is the permeability, a constant which depends on the medium alone, independent of the fluid. Thus k is determined by measuring the flow rate for a given pressure gradient or vice versa; the fluid viscosity and sample length must be known in advance.

One may also speak of a fluid diffusivity, c, defined, as with thermal diffusivity, by the following equation:

$$c\nabla^2 P = (\partial P/\partial t) \tag{1.2}$$

It can be shown that c is proportional to $(kK_f)/(\mu\Phi)$ [Cleary 79], where K_f is the bulk modulus of the pore fluid and Φ is the porosity. This diffusivity term has units of $(\text{length})^2/\text{time}$. The decay of pressure in a semi-infinite

porous medium, where the pressure at the boundary is instantaneously zero, may be expressed roughly as a one dimensional first term of a series of error functions describing the decay in pressure along the direction x as:

$$(P/P_i) = \mathrm{erf}\left(\frac{x}{\sqrt{2ct}}\right) \tag{1.3}$$

By measuring the time for a small pressure decay, for example, across the lenght of sample of known dimensions and bulk properties, one may therefore indirectly estimate the permeability of the material.

The samples used in this test are approximately four inches in diameter and from two to four inches in length. This squat design allows good ultrasonic measurements along the axis, while allowing the fluid to flow in or out of the sample in the radial direction. The changes in the pressure within the sample are complicated by the endcaps for ultrasonics measurement. The endcaps do not allow the pressure to level leak off in the axial direction, thereby complicating the diffusion of pressure out of the sample.

The bounded diffusion solution in time and in all directions for our sample is a superposition of the steady state pressure throughout the sample, a Bessel function solution for the radial direction and a Fourier sine series approximation in the axial direction. The derivation of the solution is beyond the scope of this treatment, but the general trends of pressure gradients are sketched in figure 1-1.

The radial solution would be of the form:

$$P(r,t) = P_0 - \frac{2P_0}{b} \sum_{n=1}^{\infty} \frac{e^{c\alpha_n^2 t}}{\alpha_n} \frac{J(r\ \alpha_n)}{J(b\ \alpha_n)} \tag{1.4}$$

where b is the radius of the cylinder, r is the fractional distance along

the radius and α_n are the eigenvalues. The complete details of the diffusion analysis are presented by Fitzpatrick, 1983, including the distibution of stress as caused by the excess pressure within pores. For our purposes the solution in eq (1.4) combined with the approximate solution axially, as in heat flow is:

$$\sum_{n=0}^{\infty} a_n \sin\{\frac{n\pi z}{l}\}\exp(\frac{-n^2\pi^2 ct}{h^2}) \tag{1.5}$$

where n = (1,2,3...)

The Fourier coefficients, a_n, are determined in the usual manner, allowing the superposition of these two solutions to demonstrate that the pressure drop from the center of the sample is contributed to by both the excess pressure by the bounded edges as well as from the radially symmetric diffusive flow.

The gradients are approximated by figure 1-1 which shows the general trend of the pressure gradients incurred by induced overpressuring. The totally destroyed samples actually show fracture patterns similar to this.

On the microstructural level the sample, in this case a mortar form of concrete, incurs damage in the form of cracks in the connective matrix along preferred prefractures. Throats of connective pores leading into thin cracks which are partially cemented would be enlarged by the overpressuring of the pore space. Grain boundaries and other interfaces may be forced apart by the pore fluid. In section 2.3 cracks of angular nature are seen propagating throughout the sample. The number, or density, of cracks increases as well as the length of the cracks increases during the induced pore pressure fracture

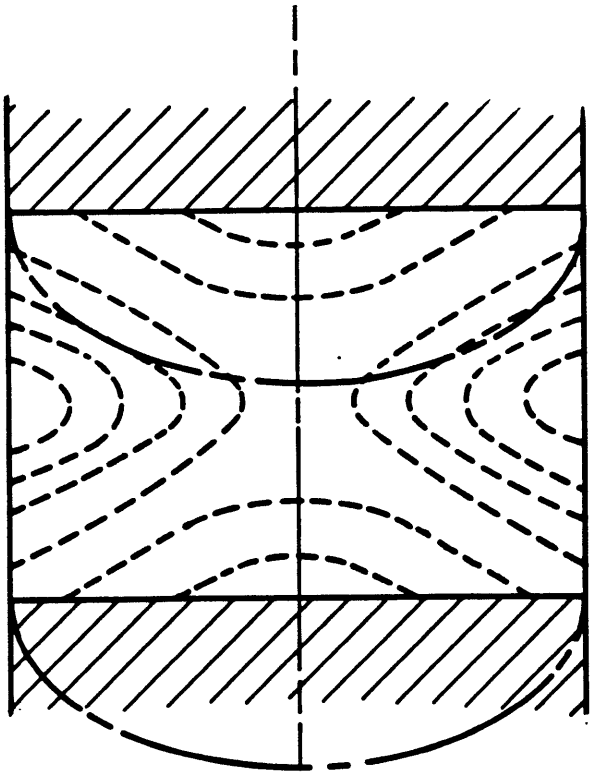

Figure 1-1: Sketch of pore pressure distribution at some time after loss of confining pressure. (After Fitzpatrick, 1983)

event.

The creation of many small cracks will change the physical properties of the material, but the influence that the cracks have on the properties depends on the behavior of the cracks themselves. Orientation, shape, surface contacts, concentration, and the fluids within them are a few of the parameters that control cracks. In this study the use of ultrasonic velocity and attenuation will be sensitive to two factors . 1)The attenuation is indicative of the number of saturated cracks and the degree to which they are saturated . 2)The compressional and shear wave velocities are also sensitive to pore space saturation and crack density. [Winkler and Nur 79] [O'Connell and Budiansky 77] [Walsh and Grosenbaugh 79] [Stewart et al 80] [Cleary 80]

1.2 Pulse Transmission Methods

Many inherent problems are encountered when measuring attenuation with the wave propagation method. In addition to intrinsic damping, geometric spreading, reflections, scattering due to poor coupling at interfaces, and material inhomogeneities may all cause signal loss. These problems are overcome by measuring wave amplitudes on a reference sample with low attenuation characteristics. These values are then compared to the samples under the same conditions and attenuation is thereby determined by comparison of the spectral ratios. This technique has been previously employed. [Toksoz, Johnston and Timur 78]

One can expresses the amplitudes of seismic waves in the form

$$A_1(f) = G(x)\ e^{-\alpha_1 f(x)}\ e^{i(2\pi ft - k_1 x)} \tag{1.6}$$

$$A_2(f) = G(x)\ e^{-\alpha_2 f(x)}\ e^{i(2\pi ft - k_2 x)} \tag{1.7}$$

where 1 and 2 refer to the reference and the sample respectively, A is amplitude , f is frequency , x is distance , k is the wavenumber ,v is the velocity, G(x) is a geometrical factor which includes spreading and reflections, and α_1 is the frequency dependent attenuation coefficient.

This method *a priori* assumes that alpha is linear over the considered range of frequency. Fortunately, available data suggests that this assumption is true. [Knopoff 60] [Jackson and Anderson 70andAnderson] [McDonal 81] This

then allows one to write,

$$\alpha = \gamma f \tag{1.8}$$

assuming gamma to be constant the relation to the quality factor is

$$Q = \frac{\pi}{\gamma v} \tag{1.9}$$

For the application of this technique, the reference and the samples must have the same geometry. Similar techniques were used to ensure uniform and reproducible coupling to the sample . One can then assume the terms G_1 ,G_2 to be frequency independent scale factors. The ratios of the discret Fourier amplitudes afe then:

$$A_1/A_2 = G_1/G_2 \quad \exp^{-(\gamma_1-\gamma_2)fx} \tag{1.10}$$

$$\ln A_1/A_2 = - (\gamma_1 - \gamma_2)fx + \ln G_1/G_2 \tag{1.11}$$

where x is the sample length. If the assumption that G is independent of frequency is correct, then the slope of $\ln(A_1/A_2)$ will be the 'gamma factor ' from equation (1.8). Having found the Q of the reference material, the γ_2 of the sample then can be determined. Following Toksoz, Johnston and Timur (1978),this technique calls for Q to be very high such that γ_1 is approximately zero and γ_2 can be directly determined.

Aluminum is used as the reference material . The measured value for the Q of Aluminum is about 150,000 [Zamanek]. This gives an α for aluminum which is approximately zero. Measured values of Q for typical rocks are generally in the range of 10-100. This allows less than .1% error in the measurment of Q.

Experimentally, the concern over the assumption of the frequency independence of the geometric factors G_1 and G_2 can be eliminated by repeated collection of pulse shapes and amplitudes from similarly prepared samples. As well, examination of the reflection coefficients, shows no apparent frequency dependence from well coupled, flat, and parallel interfaces. The terms for an anelastic solid may include complex moduli but as can be seen from the above technique, no matter what the ratio of transmission coefficients the slope of the curve is independent of the intrinsic loss coefficient.

For the purposes of this study, the examination of attenuation is limited to regions of frequency over which interference from reflected waveforms and low frequency baseline disturbances are minimized.

Chapter 2
Experimental Techniques

2.1 Ultrasonic Measurement System

An ultrasonic measurement modeled after systems developed at MIT by Karl Coyner and David Johnson was developed for this study. The system measures velocities and attenuation by the "pitch and catch" wave propagation method. Signals are sent and received using similar piezioelectric transducers (PZT-5) then captured and digitized on magnetic disk and subsequently analyzed.

A block diagram of the systems electronics appears in figure 2-1.

A Panametrics model 5055PR pulser-receiver unit provides uniquely matched electrical pulses to the transducers as well as acting as as an amplifier for the received signal. The 5055PR unit also simultaneously sends a timing trigger signal to the Nicolet-III digital scope. The digital scope has a sampling rate of .5 micro- seconds, allowing accurate resolution of signals at or below one megahertz. The Nicolet-III also stores and transfers data on floppy disks, allowing direct computer manipulation of the digitized signal.

A high-low band pass filter proved to be useful in analyzing the effects of various coupling schemes as well as in allowing the removal of spurious signals. The filter was not used in data analysis.

The geometry of the sample arrangement is shown in figure 2-2.

The samples are typically 4 inches in diameter and approximately 5 centimeters in length. This geometry has the advantage of passing waves through a large representative area of the test material, and as determined by grain size are large enough to be an elementary volume. The squat shape of the sample also eliminates the concern over sidewall reflections which can add into the straight path plane wave. Examination of the dispersional

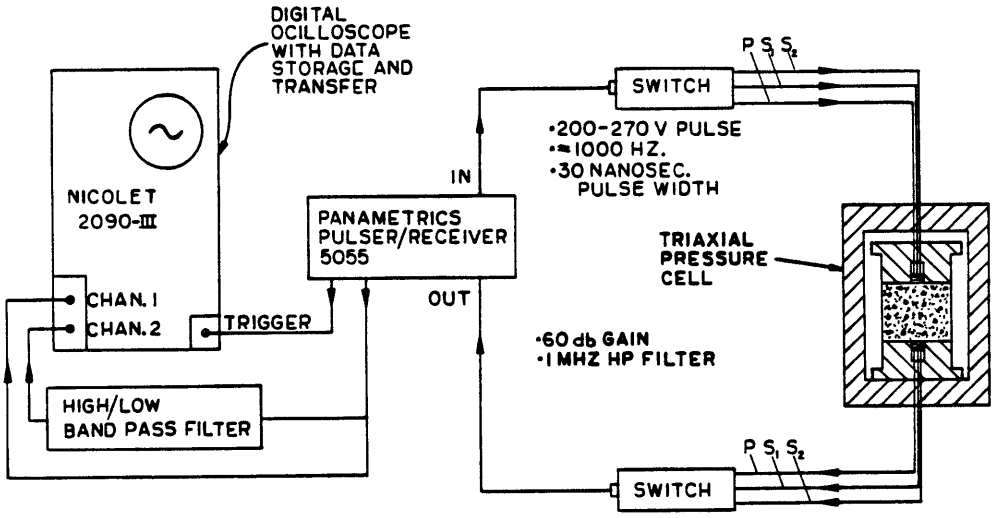

Figure 2-1: System Electronics for Measurement of Ultrasonic Velocities and Attenuation

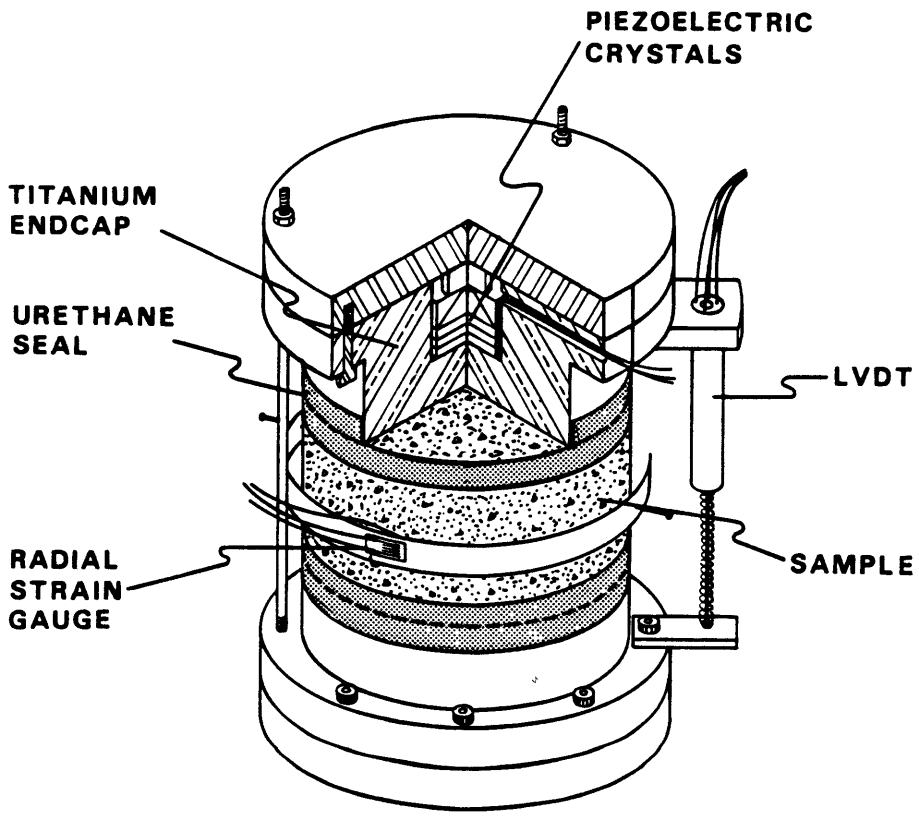

Figure 2-2: Ultrasonic Measurement System Sample Geometry

characteristics reveals that [Tu 55] the criteria for clear compressional wave arrival requires the length-to-diameter ratio to be less than 5, whereas this systems is about 2. Further the diameter-to-wavelength ratio must be greater than five to minimize dispersion. Scattering effects, which can become significant when the grain size is about one third the wavelength examined, are also eliminated. (λ = 0.5mm, G_s = .01mm)

The crystals used in this study are lead -zirconate titanate (PZT-5) with compressional or shear capablities . The combined transducers are stacked similar to [Coyner 83] figure 2-3. Both receiver and sender have equivalent characteristics with centered resonant frequencies at two megahertz. Waves are selectively propagated (Compressional or Shear) by excitation of appropriate potentials in the stack.

The backing on the stack of transducers is designed to reduce reflections such that all of energy is propagated to the sample. PZT-5 without a prefered crystalographic orientation is bonded to the back of the transducer stack in a conical shape. The cone channels the side wall reflections, causing them to cancel each other out or deflecting them into a lead-epoxy damping material surrounding the cone. Figure 2-3

Titanium endcaps are used to place the transducers in an environment isolated from pressure, which serves to provide constant coupling. Several reasons are apparent for the choice of titanium. First, endcaps made from titanium have a similar acoustic impedance to many earth materials, allowing for an effective transmission of waves accross the interface between the sample and the endcaps. Secondly, the titanium resists deformation at elevated pressures, allowing the assumption of flat and parallel interfaces to remain valid.

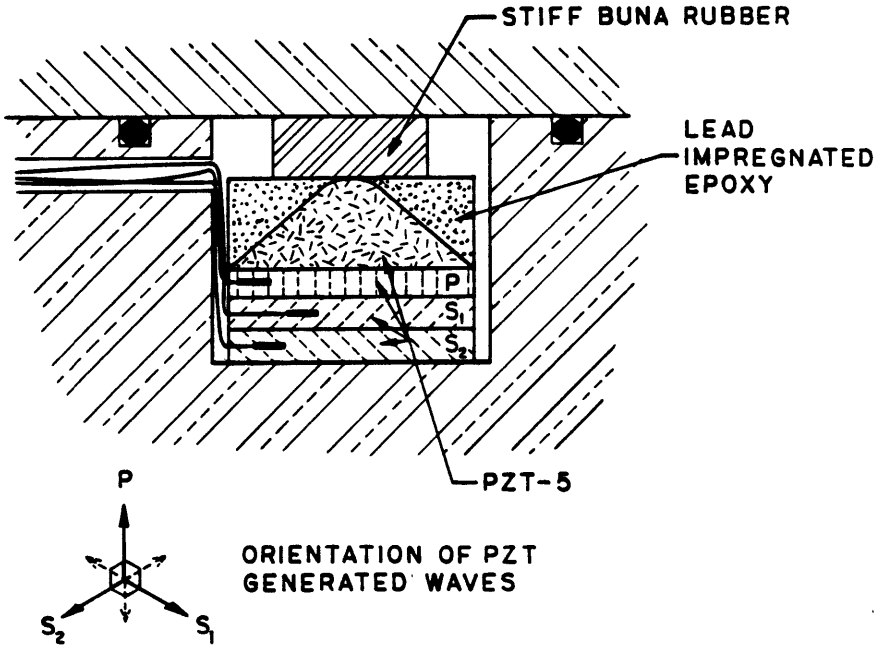

Figure 2-3: PZT-5 Crystals with Lead Epoxy Backing

2.1.1 Velocity Determination

Velocities are determined from the wave propagation method by first obtaining the total system delay time ΔT_s. The intrinsic delay is a combination of several factors including transducer characteristics, endcap material and thickness, and electronical delays. Determination of ΔT_s can be accomplished by several techniques. The first, and most obvious, method is to place endcaps face to face, allowing only the effect of a cleanly coupled interface to interfere with signal transmission. This method may not fully simulate signal transmission due to the lack of acoustical contrast, which band shifts the frequencies.

A second method used is determining the effective zero length time delay, progressively shorter lengths of Aluminum are used to standardize the delay of the first arrival versus time under experimental conditions. The arrival times can be projected back to zero length thereby determining ΔT_s

The simple equation;

$$V = \frac{L}{\Delta T - \Delta T_s} \tag{2.1}$$

defines the velocity as determined by the sample length, time of arrival signal, and total system delay time. By using the above equation, the delay time at zero can be graphically determined.

Picking a first arrival is classically defined as the first deviation from noise at the beginning of a recognizable waveform as shown in figure (2.1) with an ordinary P wave. Errors can be encountered by the picking of such a deviation from noise, but this effect is minimized by consistent and

repeated methods for the determination of the first arrival. With the resolution of .5 microseconds per point and the typical velocities encountered in this study, have been analyzed for the error in velocity determination acheiving an error below 2%. [Gregory and Gray 76]. This error can be effectly corrected by the use of a curve fitting program and various filtering schemes which allow greater confidence in picking the first arrival.

During the experiment, sample length is determined by a LVDT with a resolution in the microstrain region. (See figure 3-4. The change in length with time is applied to velocity-time relationship to eliminate errors due to axial strain.

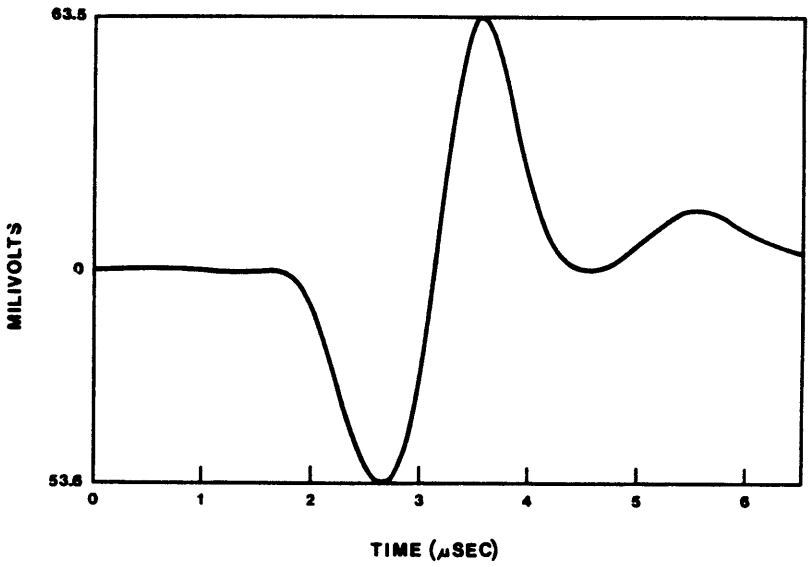

Figure 2-4: Typical First Arrival Of Sample Waveform

2.1.2 Attenuation Measurement

The study of intrinsic attenuation is a complex and difficult task. Many factors contribute to the reception and transmission of ultrasonic waves. Signals are decayed by many contributing phenomena which can cause erroneous attenuation. Using the mathematical methods outlined in section it can be shown that the development of a consistent procedure for attaching of the samples to the endcaps' surface for consistent acoustical coupling allows the determination of intrinsic attenuation in this system.

Waveforms are collected after passage through the sample, are digitized and are then stored on magnetic disk directly with a digital oscilliscope. The resultant waveforms are influenced by the input pulse from the Panametrics pulser-receiver, the amplification , and the various filters built into the system. The settings used for each of these subsystems were standardized so as to compare sample to sample and to the reference sample, aluminum. The methods in section show that the comparision to aluminum is vital to gain the frequency dependent coefficient of attenuation α . Over the range of frequency studied, the geometrical effects are eliminated by the use of the techniques in section .

The waveforms are then transfered directly to a lab computer, a Digital Equipment Corporation's MINC-11, by an IEEE-GPIB standard interface. The waveform is stored on a large floppy disk and analyzed. The collection system is driftless due to the precision with which waveforms are collected and recorded. The pulser system may vary in it's output and must be kept at a warm state for the duration of the experiment.

The generation of the waveforms varies slightly on the baseline voltage, but the absolute amplitudes are unaffected.

The waveforms are decomposed into their component frequencies using a discrete Fourier transform routine. The amplitudes over the range of frequency investigation are studied with respect to the no-loss material, aluminum . The ratios of the discrete amplitudes are obtained simply by straightforward comparison of the amplitude data.

2.2 Error Determinations

The most crucial area in the wave propagation method is the interface between the endcap and the sample. Slight deviations from parallel cause additional losses from the creation of higher energy reflections. Flatness of the sample is just as crucial to the transmission of waves. "Dished" areas of contact cause actual losses in physical contact thereby reducing the transmission by a factor directly related to the connected region.

Techniques used for this study included careful preparation of both the samples and the standards to ensure flatness and parallelicity. The samples were surface ground to within one thousandth of an inch parallel with a diamond wheel. The error due to the shaping of the specimens is less than one-half a thousandth of an inch in length. The flatness was better than 40 microns.

Coupling was kept constant from sample to sample through the use of silver foil, which is both similar in acoustic impedence to the system and malleable enough to mold itself to smooth out any irregularities in the surface.

Each system that measures Q uses several linked electrical devices each of which has associated delays and nonlinearities. The received data will be altered by this complex interaction which must be known in order to know the accuracy of the attenuation measurement. The equipment was determined to have a low level of inaccuracies from the repetition of aluminum samples. Discrepencies were apparent from "cold" starts of the pulser-receiver or the digital scope. This problem was minimized by keeping all the equipment at "warm" states during the course of the experiment. Errors in Q caused by the change in amplitude due to variables within the electronic system amounts

to less than 2% for waveform amplitude but up to 10-15% error for Q. This figure for the system is comparable to others. [Johnson 78].

2.3 Fracture Technique and Sample Preparation

Observations of the physical properties of the test material, a mixture of Portland cement, quartz sand, and water, has allowed development of a fracture technique which is identified as pore pressure induced fracture. Pressure distributions and stress concentrations follow the analysis in section two, although the technique here inherently assumes that the system is both fully saturated and at equilibrium prior to the pressure drop. This assumption is physically realized by the use of both the ultrasonic system and strain gauges which allow the monitoring of the change in properties apparently due to to the saturation of the sample.

The oil cement system is assumed to be inert. Analysis of the interaction of the mixture of Portland type II cement, quartz sand, and water appears to have been extensively studied in the construction engineering literature. [Neville 80].The compounds formed are on the low end of the diagenetic scale with many comparable calc-oxide polymorphs that may react with quartz to form many well recognized compounds.

It has been assumsed, by comparing the compunds involved, that the interaction between the oil and cement compounds is neglectable. This would not be the case as with water, as can be readily seen from examination of the same criteria.

The inertness of the system to chemical interaction has been quantified by noting that at constant pressure and saturation, neglectable drift with comparison to instrument drift was observed.

The ratio of sand to cement in the material used in this study was formed is about equal. The microstructural aspects of this compound show a

high degree of columnar overgrowths between well rounded grains. The matrix is very well cemented with natural cracks and pores occuring in a uniform manner. The destruction of the microstructure appears to advance from the saturated pore space.

This material was chosen for it's low tensile strength and relatively high diffusivity, which would accent the pore pressure fracture phenomena based on a concurrent study of diffusive fracture. As well, addition studies on hydraulic fracture use similar compounds and the use of the cement material allows comparison of experimental results on a relatively homogeneous , well studied, and easily acquired material.

The sample is first slowly pressurized, to avoid damage by crushing of unsaturated regions, and allowed to saturate. Once a stable condition has been reached, determined by the ultrasonic velocities and strain gauges, the outer pressure is dramatically reduced, causing the pore pressure to exceed the confining stresses. The fluid does, by nature of the jacketing scheme (figure 2-2), move out of the sample; however, as it has been shown the sample should remain at a high degree of saturation.

Unlike previous experiments with wave propagation systems, the sample in this experiment is semi-jacketed. This allows the fluid flow in and out of the exposed annulus on the sample while maintaining constant coupling at the sample endcap interface. The area where the endcap is in contact with the sample is the only area completely isolated from the pressurized fluid. It is vital that no fluid come between the sample and the endcap, thereby reducing the transmission of shear waves through the the interface.

The sample configuration shown in figure 2-2 is held together by the use of stiff springs and threaded rods as well as the jacketing compound of semi-

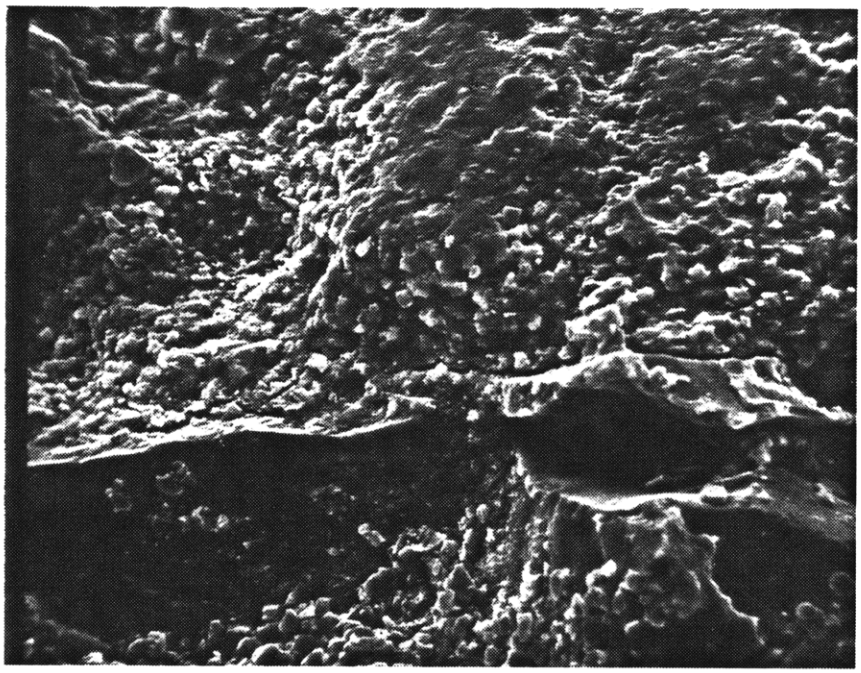

510x

Figure 2-5: Electron Microscope image of Fractures in a Virgin Sample with cracks approximately 50-100 microns long

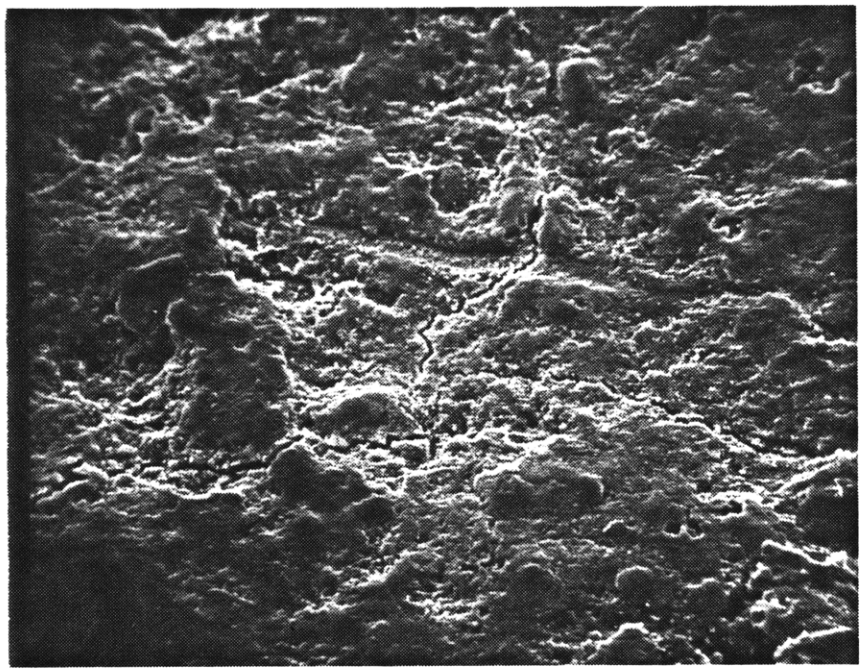

192x

Figure 2-6: Electron Microscope Image of Fractures from Pore Pressure, lengths approximately 500-800 microns

flexible urethane. The stiff springs allow the endcaps to follow the sample when it deforms, thereby maintaining a continuous level of coupling. The springs are made from large washers deformed about a spherical ball bearing forming a conical washer that acts as a spring. The technique has proven itself by showing coupling is maintained in all experimental runs of the system.

Once the sample is saturated and brought to equilibrium at a typical pressure of 9,000 PSI, the pressure is suddenly relieved in the vessel. This brings about the sudden introduction of stress gradients due to the presence of overpressured pores similar to the analysis in section . This stress is effectively tensile and should move from the saturated pore spaces into newly opened microcracks. As evidenced from the scanning electron microscope pictures the fractures do develop in number and in size from the overpressuring of the pores.

Velocities and waveform attenuation are observed during the fracture event, which usually is on the order of a few hours. The strain on the sample is observed concurrently with the velocity and attenuation measurements.

Chapter 3
Induced Fracture Effects on Velocities and Attenuation

3.1 Experimental Data

3.1.1 Velocity Change during Induced Fracture

The velocity shift during pore pressure induced fracture was observed over a number of cycles as a function of time. Pressure was cycled over a range of nine thousand psi as shown in figure 3-1. Maximum pressure was reached by a slow sucession of steps of approximately one thousand psi. Slow pressurization of the pore spaces insures that no damage due to resulting stresses from high pressure gradients can occur. After steady state was acheived, the confining pressure was released allowing the internal pore pressure to effectively bring the stresses in the sample to tensile states, according to the effective stress relationship, $\sigma^* = \sigma - p$.

As the transient tensile states exist within the rock matrix, wave velocities are found to change over that period. Velocities are seen to increase immediately after the confining pressure drop to values that increase as much as 4% as the pore pressure equilibrates during diffusive flow. Immediately after pressure drop when the sample contains the highest internal pore pressures which decay according to the laws of diffusion. The time required for acheivement of steady state values of stress and internal pore pressure is about ninety minutes or eight times τ_c, the time constant for diffusive flow in the sample. Compressional and shear wave speeds are shown in figures 3-2, 3-3 and in appendix one.

The compressional velocity shows an almost negligible change in velocity (2%) during the fracture event. Over the same period the shear wave velocity changes up to 4% over the instantaneous value. Both velocities are corrected by the axial deformation during the experiment and the intrinsic system delay.

Comparision of the velocities after the release of confining pressure show a reduction from initial saturated conditions. Typical losses are low with the shear wave speed changing less than 5% . The change for compressional velocity is less with typical changes of less than 2% .

Over several cycles the steady state velocity changes slightly as a result of the damage caused by the pore fluid, which will be dicussed in the next section. The shear velocity varies less than 2% over two cycles and less thereafter. The compressional steady state velocity varies over several cycles by 1% or less.

These numbers are just above significant levels of resolution for this system, however repetition of the experiment over a number of cycles points to a slight decrease in velocity with cycling.

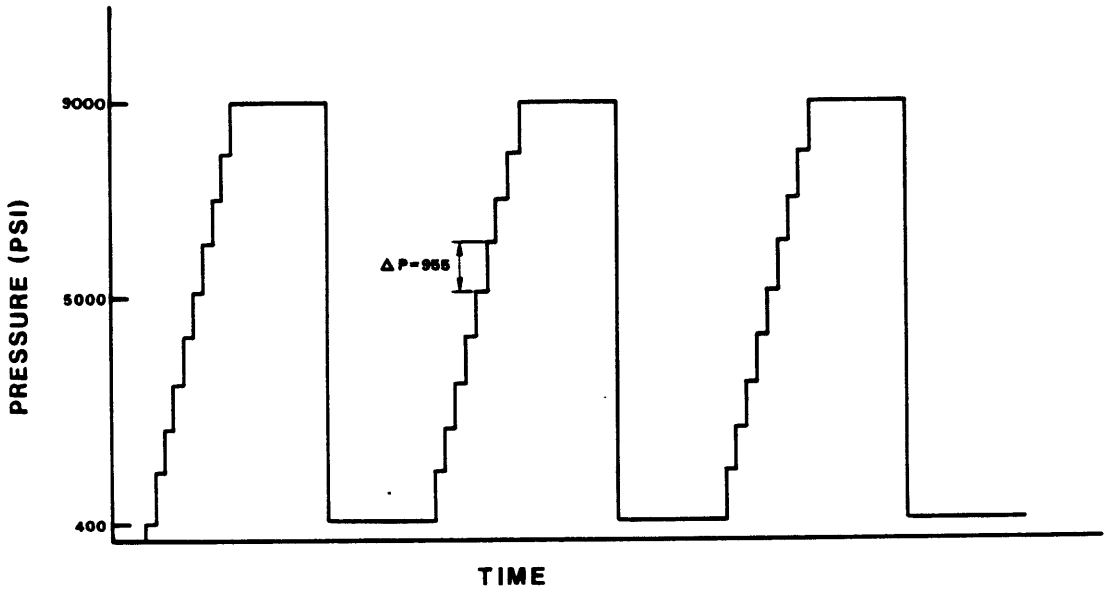

Figure 3-1: Pressure History for Cycles of Pore Pressure Induced Fracture

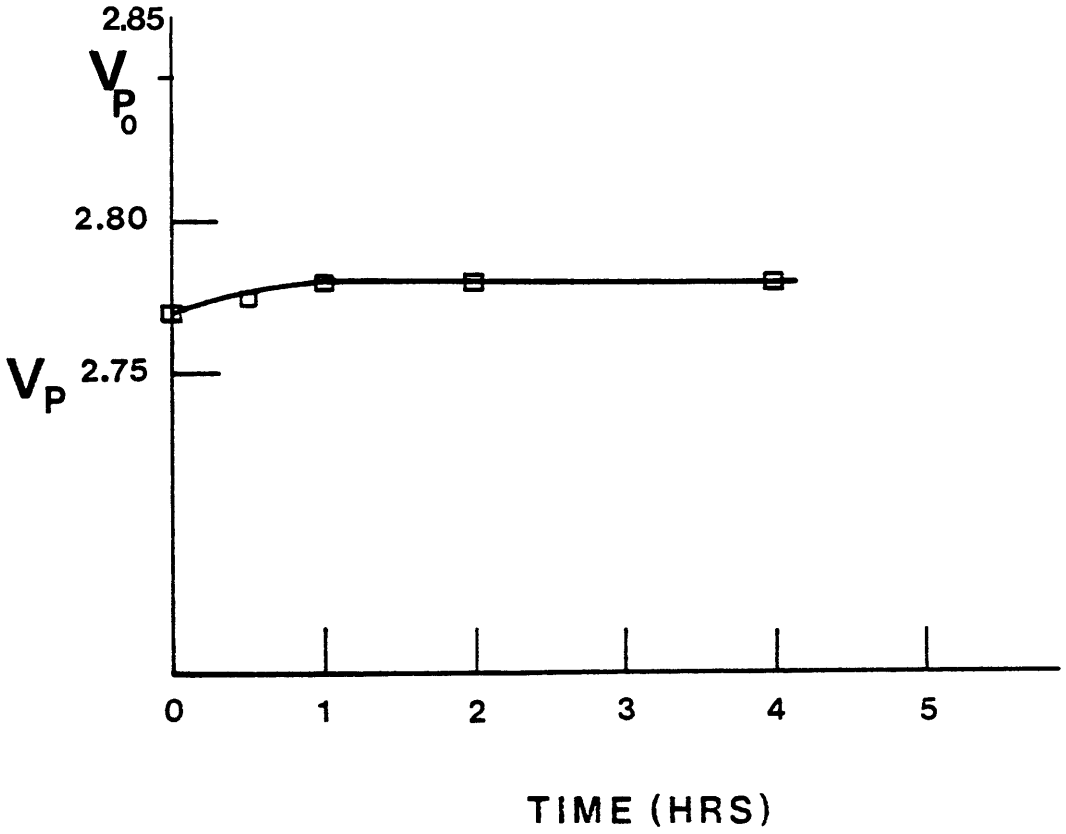

Figure 3-2: Compressional Wave Velocity During Induced Pore Pressure Fracture.

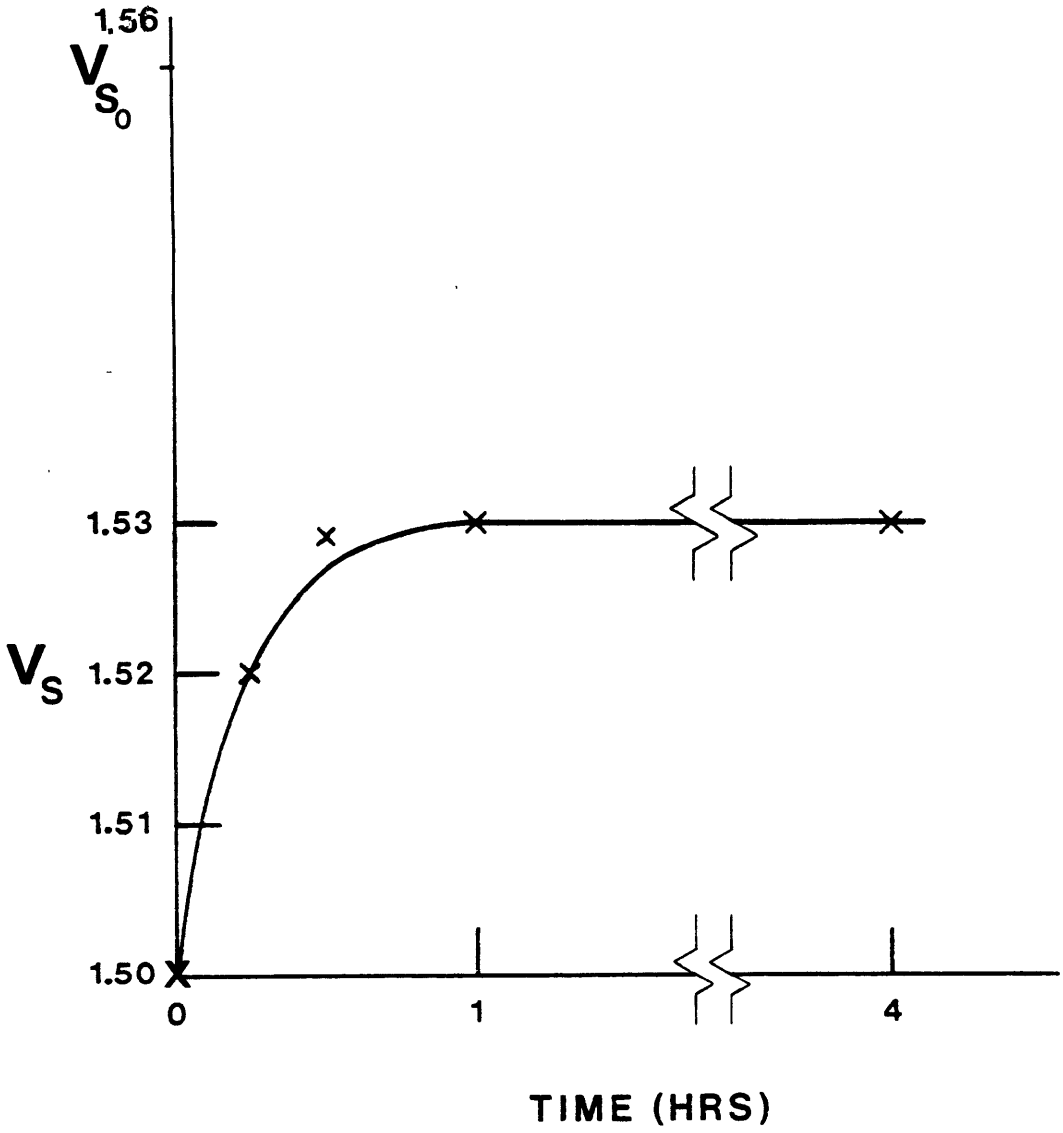

Figure 3-3: Shear Wave Velocity during Induced Pore Pressure Fracture.

3.1.2 Strain during Pore Pressure Induced Fracture

The strain incurred during the overpressuring of the pore spaces was observed in the radial and axial directions as shown in figures 3-4, 3-5 and in the appendix.

As can be seen in the figures, the strains behave differently in the radial and axial directions. The radial strain indicates that the sample expands as the pore pressure is at a maximum and then contracts, as seen in the figure, as the pore spaces reach equilibrium . There was observed a permanent deformation in the radial direction with successive cycling pore pressure induced fracture .

Radial strain of samples is measured using clip-on gauges (see Figure 2-2), eliminating the need for directly applied strain gauges. The gauges were designed so that they could be easily attached to an assembled sample stack. These gauges are more compact and are positioned easier than cantelievered beams or LVDT's.

The gauge design is constrained such that the force to expand the rings must be small enough so as to not affect the sample expansion. This force must also be great enough to maintain a clamping force on the sample which will prevent gauge displacement due to its own weight or slight disturbances in the apparatus. (After [Heintz 83])

Axial strain behaved differently than radial strain with the sample increasing in length over the period $8\tau_c$ as seen in figure 3-4 and appendix one. The sample lengthened with applied pressure and then reduced in length when the confining pressure was released only to again lengthen as the difussive pressure drops in the pores.(See appendix one)

Axial strain is frequently measured by directly applying strain gauges to

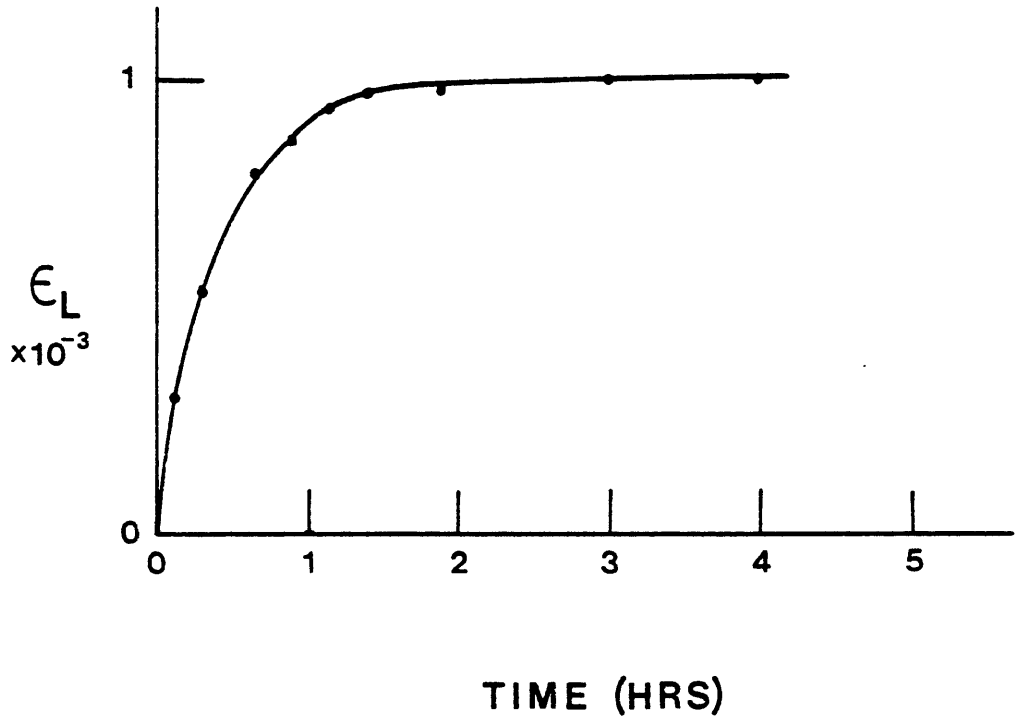

Figure 3-4: Axial Strain during Induced Pore Pressure Fracture

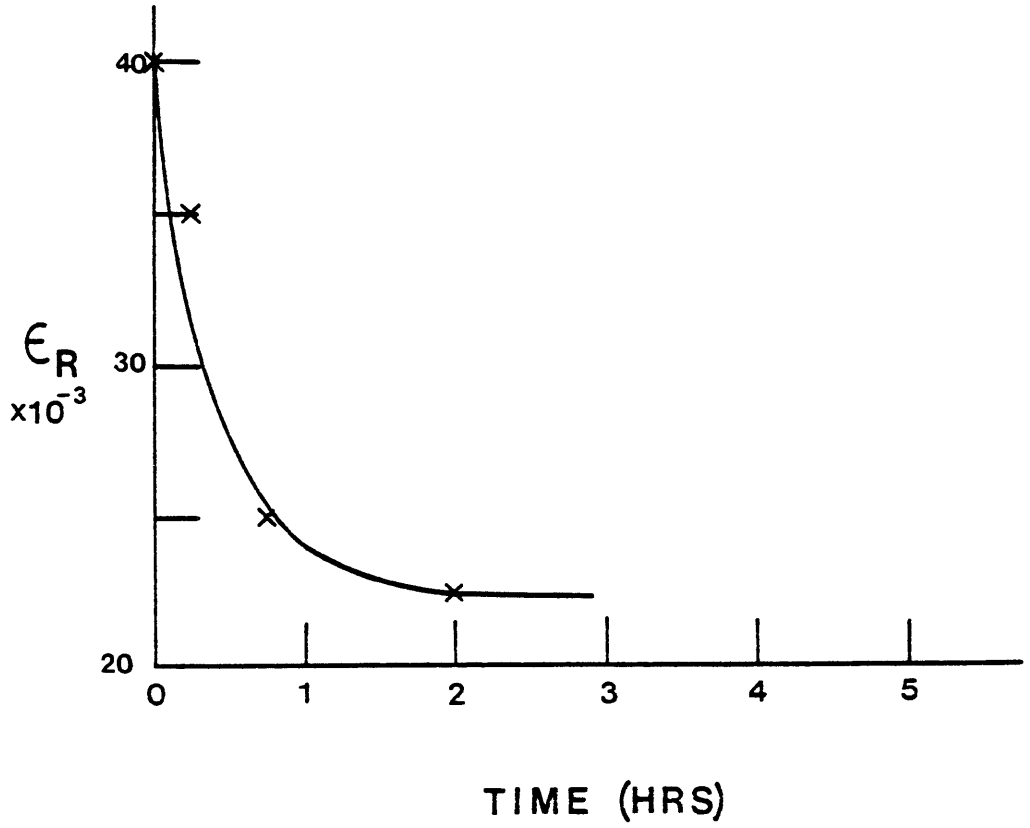

Figure 3-5: Radial Strain during Induced Pore Pressure Fracture

the sample or sample jacket. This tends to be unreliable, due to poor gauge bonding, and expensive. In order to decrease sample preparation time and increase the reliability of the measurement, A.C. LVDT's (linearly variable displacement transducers) with holes drilled in the case for pressure equalization were chosen to measure axial strain. LVDT's were chosen for their excellent resolution and stability. Conventional D.C. LVDT's cannot be used, as they contain internal electronic components (specifically, transistors) which would be damaged at elevated pressures. The A.C. transducers are identical to the D.C. ones, with the exception of the afore-mentioned circuitry is placed outside the pressure vessel.

In order to provide a secure but relatively direct measurement, the transducers are clamped to the endcaps as shown in Figure 2-2. A compensation factor for the compliance of the endcaps is only required for stiffer rocks, as the moduli for typical reservoir rocks are on the order of 0.5% to 10% that for steel. The compensation may be determined by testing aluminum samples whose modulus is reliably predetermined.

3.1.3 Observation of Wave Attenuation

The relative attenuation of the ultrasonic pulse during the pore pressure fracture event was studied over several cycles of induced pore pressure fracture. During the cycles, Q increased steadily. Relative Q changed noticeably over the period of time that the shear and compressional velocities increased. However, the detection of actual Q is difficult enough that an accurate estimate of the error in the measurement is also elusive. A worst case estimate gives a variance of about 10-20% for Q .

The number of points used in the determination of attenuation were sufficient to to avoid alaising, but the resolution after Fourier decomposition was low enough to cause concern over irregularities in the spectrum, which could not be determined with a high resolution. Individual points in the spectrum were sufficient for discrete analysis at specific frequencies. Lacking resolution in frequency space no further development of the transducer, pulser-receiver arrangement was possible. A low frequency component was present as well as some reflections that created added irregularities in the power spectrum.

Shear waves showed an increase in relative attenuation over a number of similar experimental runs. Most of the behavior in the was evident was in a region from about 650 kHz to 750 kHz which corresponds to the center frequency of the ultrasonic pulse. Compressional wave data showed opposite and more pronounced behavior during the first cycle and thereafter. Both are displayed in figures 3-6, 3-9 and the appendix, which contains fullwaveform data for a virgin sample through two cycles. Results are to be dicussed in the next section.

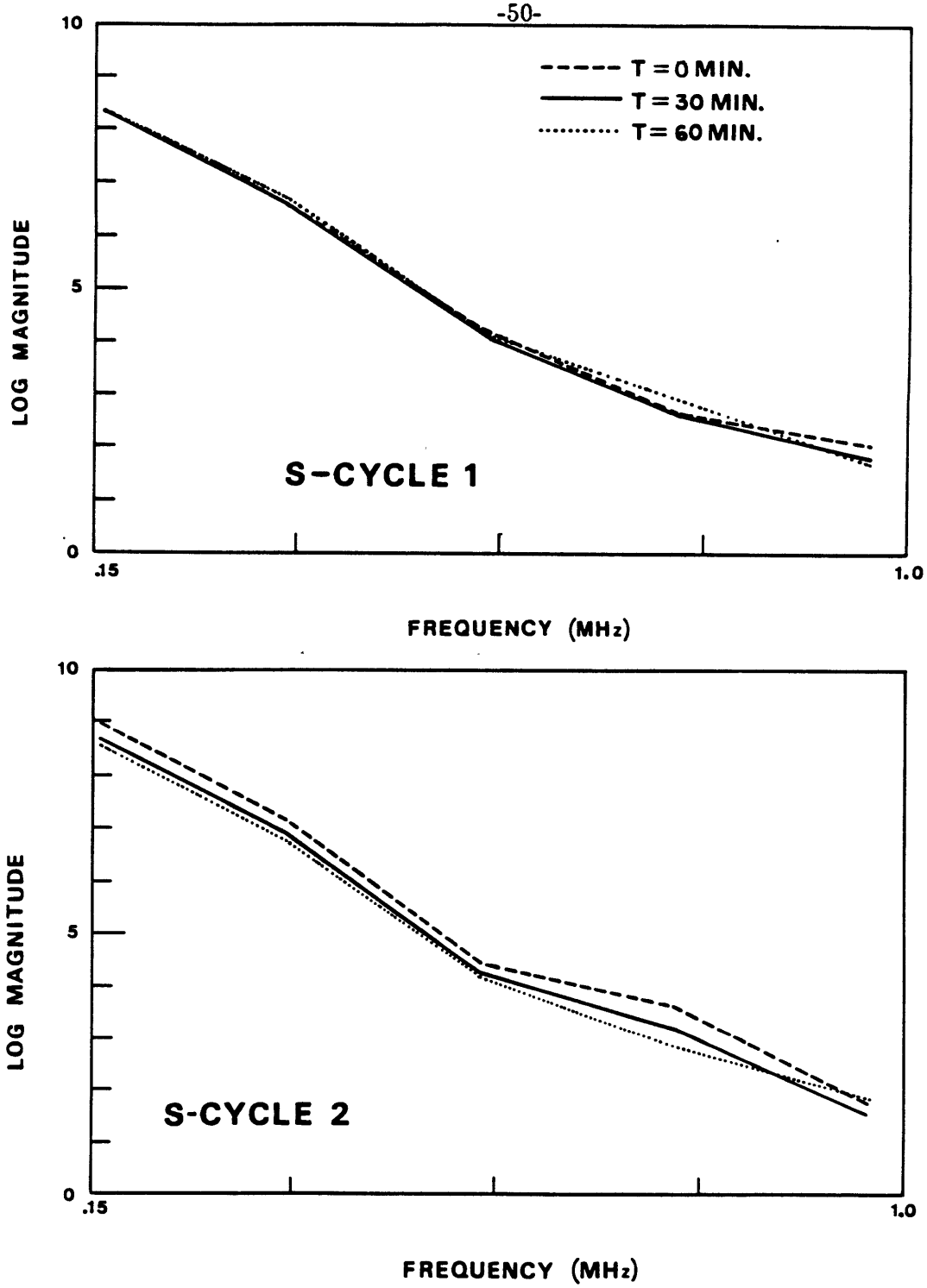

Figure 3-6: Shear Wave Attenuation

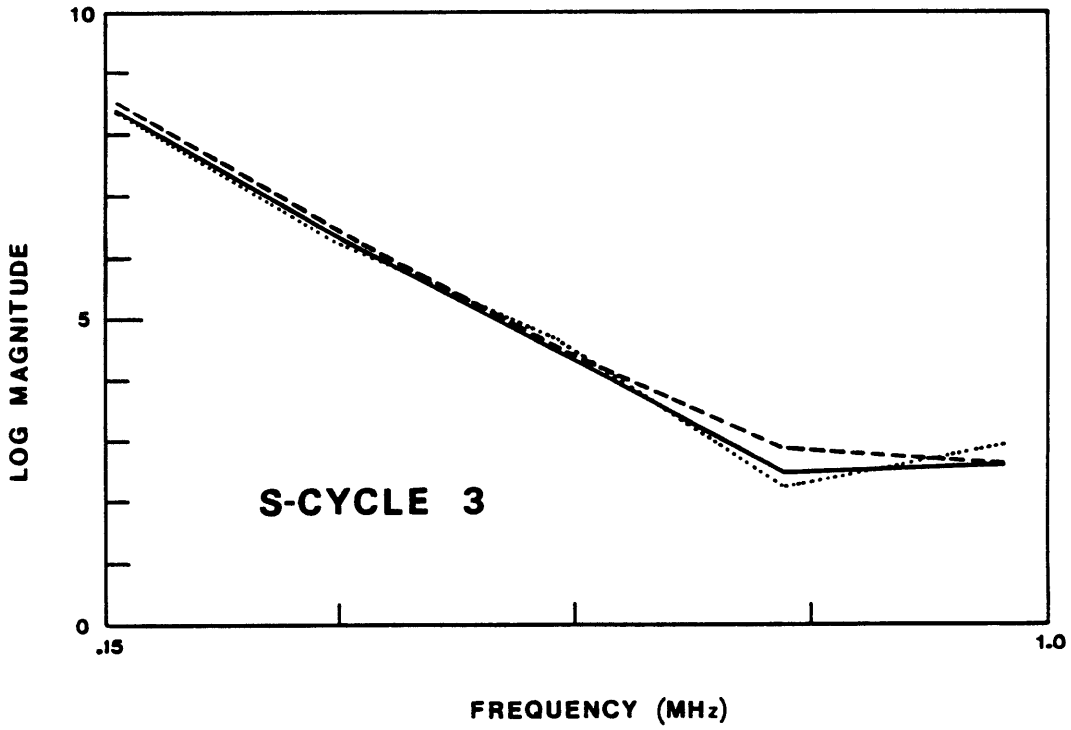

Figure 3-7: Shear Wave Attenuation

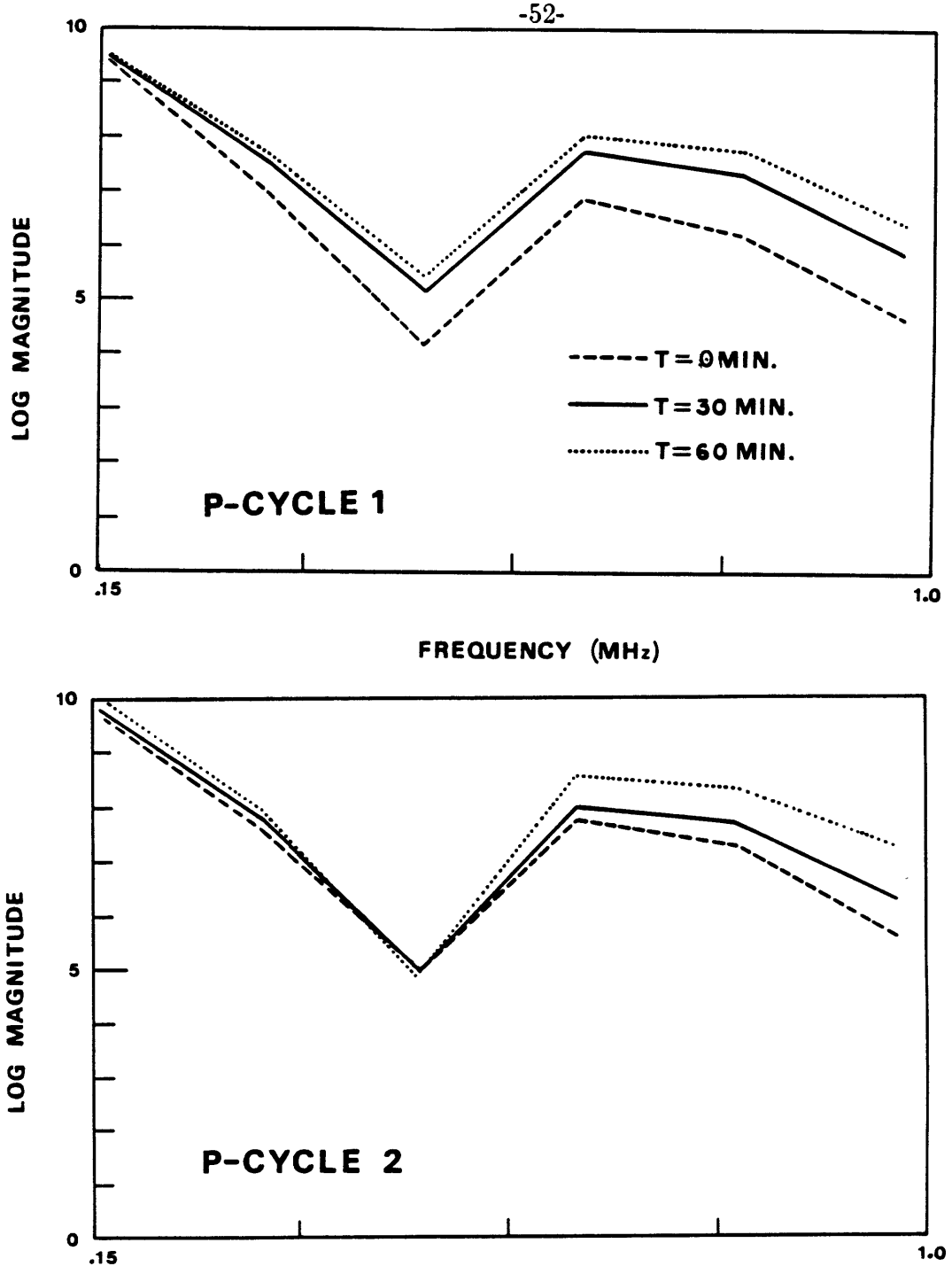

Figure 3-8: Compressional Wave Attenuation

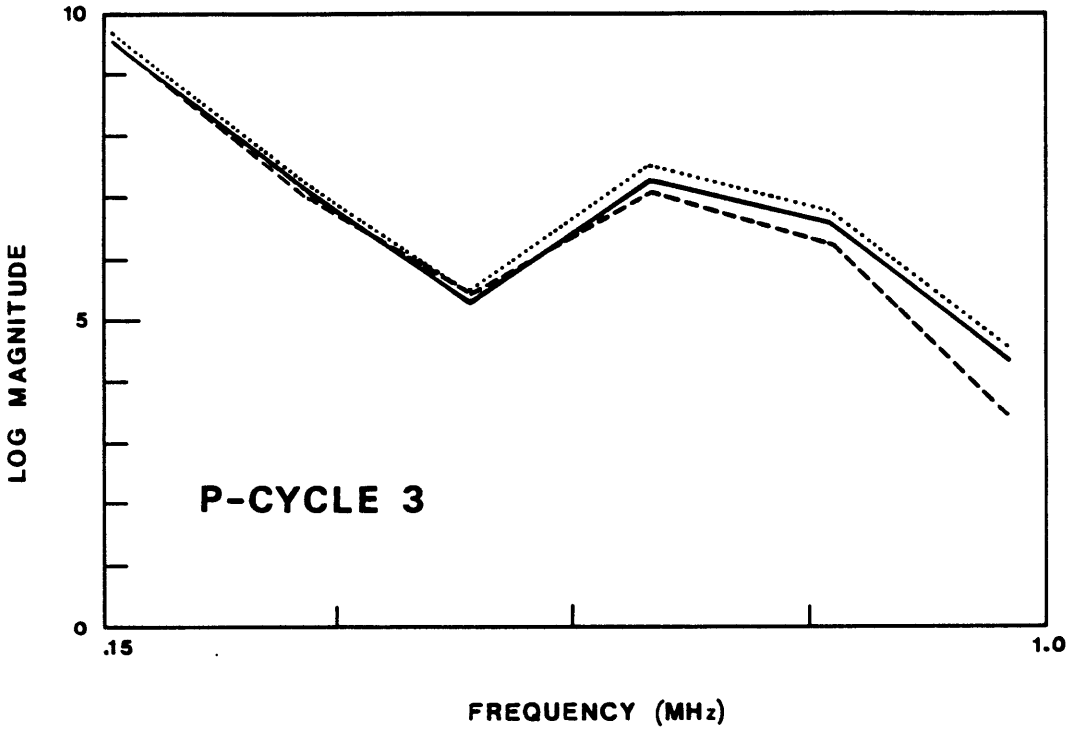

Figure 3-9: Compressional Wave Attenuation

3.2 Interpretation of Data

Data is interpreted from the results to be an observation of evolving fracture behavior on the microstructural level. Velocity shifts, strain data, and relative attenuation correspond to the scanning electron microscope observations that microcracks are formed due to the creation of effective tensile stresses by the excessive pore pressure in the experimental proceedure. In addition, data points towards the creation of two distinct types of damage to the microstructure: one having a permanent nature and the other dynamically changing as the internal pore pressure is relieved with time. As the number of cycles, increases the resulting transcient damage decreases but the corresponding permanent damage increases as indicated by the resulting attenuation and velocity changes.

3.2.1 Velocity Shifts

Figure 3-3 shows the shift of shear wave velocity after the drop in confining presssure. One can see that the velocity increases over the period of time that the internal pore pressure is decreasing, as governed by the diffussion equations previously discussed. Assuming that the saturation state is constant over time, the change in effective stress from pore pressure relief must be the major factor in determining the change in velocities. Saturation of the interconnected pore space is achieved by first drying a sample and then removing the gases in the pore spaces by use of a vacuum and subsequently pressurizing the sample with pore fluid. After the confining pressure drop, the pressure external is maintained hydrostatically at approximately 400 PSI insuring that saturation is maintained within the sample. Pore pressure is

assumsed to change with a minimum of mass flow, allowing the sample to remain at a high degree of saturation. An additional variable in the concern over saturation is the presence of gas in solution with the pore fluid. As the pressure is releived, the gas may leave the fluid and occupy space as a bubble. Experimental tests have found this effect to be minimal in several other experimental proceedures involving the same materials and pore fluids. ([Martin,R. 83])

Pressure relief from the interconnnected pore space follows the laws outlined in the section on diffusional fracture. The excess pore pressure present instantly after confining pressure drop is intrepreted as opening fractures from the pore space of the test material. This fractures are seen to follow favorable crack openings and spaces between usually cemented pores or bonded grain boundaries by forcing the connected grains apart or separating favorably oriented flaws in the grain structures.

Microcracks opened in this manner are supported by the fluid pressure and are opposed by the local strain in the matrix. The cracks opposed by the local stresses, close as the fluid pressure is reduced through time. Some cracks will open as result of the stress from the pore pressure but thereafter are favored to stay open by the local concentration of stresses in the matrix. These cracks result in the changes in velocity, attenuation and strain from uncracked saturated conditions.

Open microcracks would most significantly affect the shear velocity during the period that they are open. As these cracks close with time, the shear velocity would increase as shown in Figure 3-3 and the appendix.

Compressional wave velocity is also affected but not as radically.The P wave velocity would not be expected to be as greatly altered by the number

of open cracks([Cleary 80])

3.2.2 Strain Behavior

The distribution of stress caused by the presence of overpressured pores has also caused deformation due to the formation of cracks, some of which close during the course of the experiment, others contribute to the permanent strain. Figures 3-4 and 3-5 show evolving strain during the period of pore pressure relief. Appendix one show the total strain during the course of the experiment. Strain as a result of cycling incurs some level of permanent damage on the order of a few per cent. As expected the amount of permanent strain decreased with successive cycles of over- pressured pores and eventually reached a constant value. Dynamic strain behaved similarly to the first cycles following the same behavior throughout a number of cycles.

This behavior is consistent with the interpretation that the effects of overpressured pores cause microcracks to close as the pressure is relieved through time.

The radial strain followed a pattern consistent with the creation of microcracks. The overall strain was expansive and reduced through time as the pore pressure dropped. There was some amount of permanent strain possibly due to the existance of cracks.

The axial strain shows expansion with the application of pressure. With relief of confining pressure the sample shrinks back toward it's unstrained value and then expands again with the resulting relief of pore pressure. The loss of radial strain is coupled to the lengthening of the sample in the axial direction. The radial strain is larger by a factor of ten, and may have some influence on the axial values.

The larger gradients of pressure in the radial direction may cause the creation of more cracks oriented so as to give a larger strain in the radial direction. Aside from different pressure gradients the effects of the endcaps and the restraining bolts may have also had a slight affect.

3.2.3 Relative Attenuation

The use of attenuation data in the interpretation of the effects of pore pressure induced fracture at pressures of 9KSI is useful for this experiment to describe the general physical state of the material.As well, the change in the waves amplitude may be used to interpret the various mechanisms of attenuation that are influencing the material. The term relative attenuation here is used to describe the change in waveform amplitude transmitted through a sample during the course of an experiment. The advantage is obvious: no real attenuation values are used but rather values of the change in amplitude qualitative yet sensitive measure of the the effects of pore pressure induced fracture.

The determination of attenuation is a complicated multistep process. Difficulties are found when real attenuations are computed. The change in actual attenuation is below the resolution of this experiment, due to the rather low pressures acheived and the damage caused by the pressure.

Relative attenuation decreased within the period $8\tau_c$ (the diffusive time constant) and displayed less of a dynamic nature as the number of cycles increased. Relative attenuation of both the shear and compressional wave amplitude decreased with time, indicating a change in the material properties of the specimen. The closure of cracks through the period $8\tau_c$ would indeed lower the attenuation of waves propagating within the material and most dramatically of shear waves.

As shown in figures 3-9 ,3-8, 3-6 ,3-7 and the appendix, the amplitudes of the waves are shown to be changing with time. As the number of cycles increases, the changes in amplitude becomes less and less. This may be the result of the formation of new cracks with each new cycle. These new cracks

becoming less numerous due to the limited available pressure to cause more damage. One may expect, if the experiment where carried out for a much longer time, that the relative attenuation of the waveforms would eventually remain unchanged. The permanent damage at that point would be constant, and repeated cycles of pore pressure would not create more cracks unless the pressure increased beyond previous values.

As can be seen from the figures presented in the data (figures 3-9, and 3-8) the relative attenuation has a more pronounced affect on the compressional wave over the range of frequency presented. The compressional wave increases in amplitude as the pore pressure lessens over a number of cycles. This may indicate that the mechanisms that attenuate the compression wave are lessening with time. In the interpretation here, the closure of cracks filled with fluid will indeed cause the increase in relative amplitude with time as less fluid is moved from the smaller volume of open cracks.

The shear wave behaves differently, decreasing in amplitude with time. The figures 3-6 and 3-7, show the decrease of the higher component frequencies with the spectrum of the shear wave. The mechanism that is most likely controlling this affect is the creation of more and longer cracks by the over-pressured fluid which scatters the shear wave. As the cycles increase the waveforms become more stable, indicating as with the compressional wave attenuation that the number of cracks possibly scattering the wave is not increasing beyond a set level.A small tendency is seen for the attenuation of the higher frequencies over the lower ones with time for the shear wave.

Waveforms are displayed in Appendix 1 and show the shape of the pulse as the micro-fracture occurs.

References

[Cleary, 78] Cleary, M.P.
Elastic and Dynamic Response Regimes of Fluid-Impregnated Solids with Diverse Microstructures
Int.J.Solids Structures,14: 795-819, 1978

[Cleary 80] Cleary, M.P.
Wave Propagation in Fluid-Infiltrated Porous Media: Some Review and Analysis.
Technical Report, M.I.T., 1980.

[Coyner 83] Coyner, K.
in progress.
PhD thesis, M.I.T., 1983.

[Fitzpatrick, 83]
Fitzpatrick,R.
Pore-Pressure Induced Cracking and Fluid Flow in Cemented Sand Models of Rock.
Masters Thesis, M.I.T.

[Gregory and Gray 76]
Gregory, A.R. and K.E. Gray.
Progress Report on Studies of Ultrasonic Velocity Method Systems.
Technical Report CESE-DRM 61, University of Texas, Austin, June, 1976.

[Heintz 83] Heintz, James Aaron.
The Determination of Poroelastic Properties of Geological Materials and Evaluation of the Feasibility of Shale Oil Extraction.
Master's thesis, M.I.T., 1983.

[Jackson and Anderson 70]
Jackson, D.D. and Anderson, D.L.
Physical Mechanisms of Seismic Wave Attenuation.
Rev. Geophys. Space Phys., 8:1-63, 1970.

[Johnson 78] Johnson, David H.
The Attenuation of Seismic Waves in Dry and Saturated Rocks.
PhD thesis, M.I.T., October, 1978.

[Knopoff 60] Knopoff, L. and MacDonald, J.F.
Attenuation of Small Amplitude Stress Waves in Solids.
Rev. Mod. Phys. 30:1178-1192, 1960.

[Martin,R. 83]
Personal Communication.

[McDonal 81] McDonal, F.J., Angona, F.A., Mills, R.L., Sengbush, R.L., Van Nostrand, R.G., and White, J.E.
Attenuation Of Shear and Compressional Waves in Pierre Shale.
Geophysics 23:421-439, 1981.

[Neville 80] Neville, A.M.
Properties of Concrete.
Pittman Publishing Co., 1980.

[O'Connell and Budiansky 77]
O'Connell, R.J. and Budiansky, B.
Viscoelastic Properties of Fluid Saturated Cracked Solids.
J.Geophys. Res. 82:5719-5736, 1977.

[Stewart et al 80]
Stewart,R., Toksoz,M.N.and Timur, A.
Strain Amplitude Dependent Attenuation: Ultrasonic Observations and Mechanisms Analysis.
Presented at the 50th Annual International SEG Meeting, November 18, in Houston.

[Toksoz, Johnston and Timur 78]
Toksoz, M.N., Johnston, D.H. and Timur, A.
Attenuation of Seismic Waves in Dry and Saturated Rocks: I. Laboratory measurements.
Geophysics 44:681-690, 1978.

[Tu 55] Tu, L.Y., Brennan, J.N. and Saver,J.A.
Dispersion of Ultrasonic Pulse Velocity in Cylindrical Rods.
J. Acoust. Soc. Am. 27:550-555, 1955.

[Walsh and Grosenbaugh 79]
Walsh J.B. and Grosenbaugh, M.A.
A New Model for Analyzing the Effect of Fractures on Compressibility.
J.Geophys. Res 84:3532-3536, 1979.

[Winkler and Nur 79]
Winkler, K. and Nur, A.
Pore Fluids and Seismic Attenuation in Rocks.
Geo. Res. Let. 6:1-4, 1979.

Appendix 1. Waveforms and Spectra use Data Analysis

Presented are waveforms with their spectra during the first two cycles of induced pore pressure fracture. The amplitudes of the waveforms as well as those of the component frequencies are shown as they were used for this thesis.

The virgin waveforms are shown prior to the experiment at what is expected to be full saturation. The waveforms are presented over the course of two cycles displaying the effect on the ultrasonic pulse of the pore pressure fracture phenomena.

Velocity shifts for this set of waveforms are then displayed, along with the typical variance seen in the course of all experimental runs. Velocities decrease from pre-fracture states as would be expected for the formation of many microfractures as shown in a set of values displayed at the end of this section. These values are from a different experimental run and the values are not to compared to the previous set of data. Typically, velocity and the material constants varied about 10-15% for the samples.

Strain data are also presented. The radial strain shows more permanent change than the axial strain. This may be in part due to the preferential movement of fluid in the radial direction and the bounding of the sample by impermeable endcaps. The difference in pressure gradient between the radial and axial directions may account for the difference in strain.

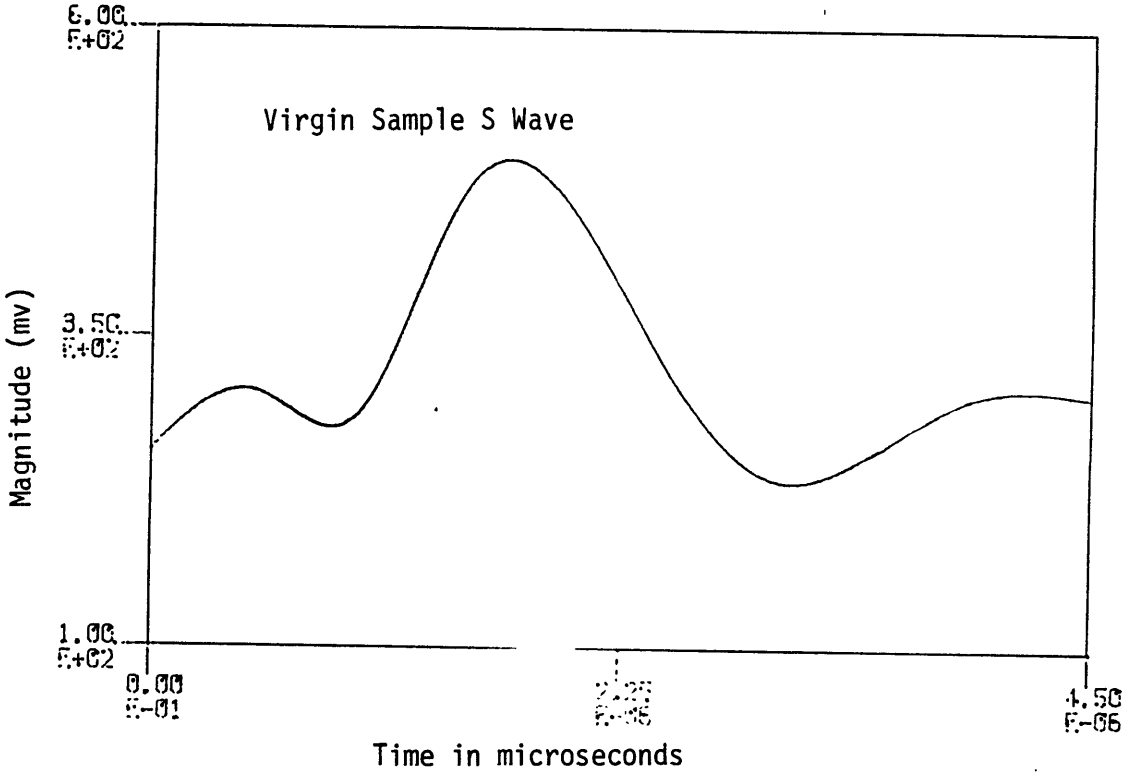
Virgin Sample S Wave
Magnitude (mv)
Time in microseconds

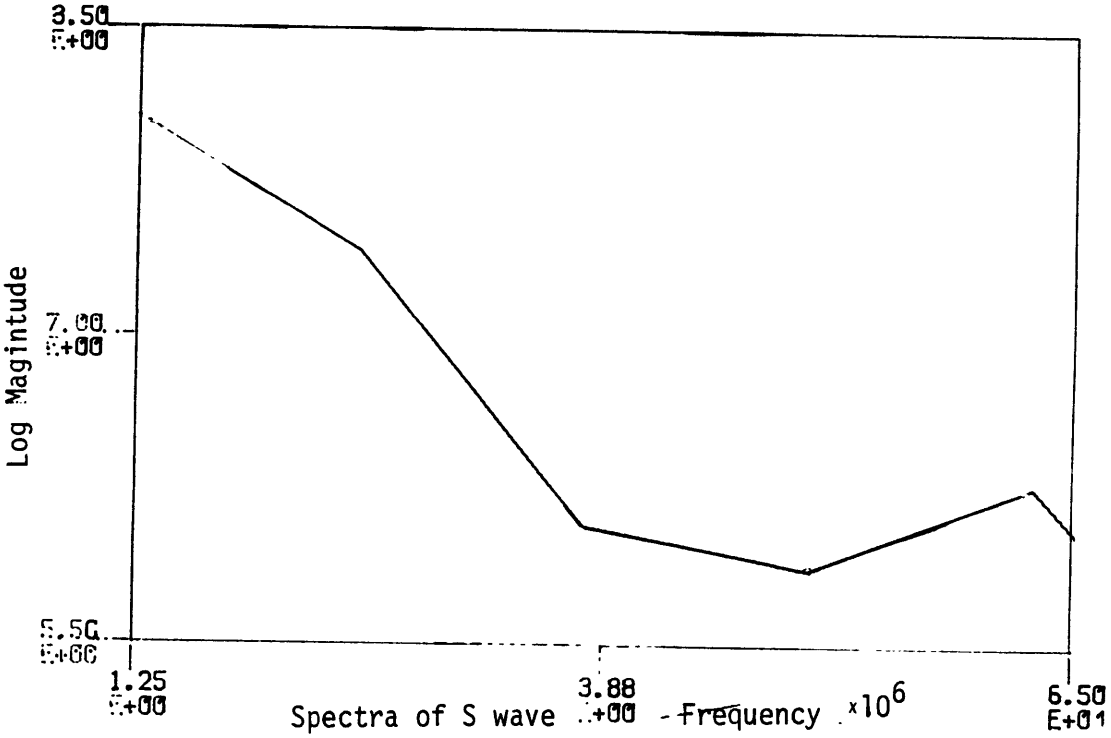
Log Magintude
Spectra of S wave - Frequency x10^6

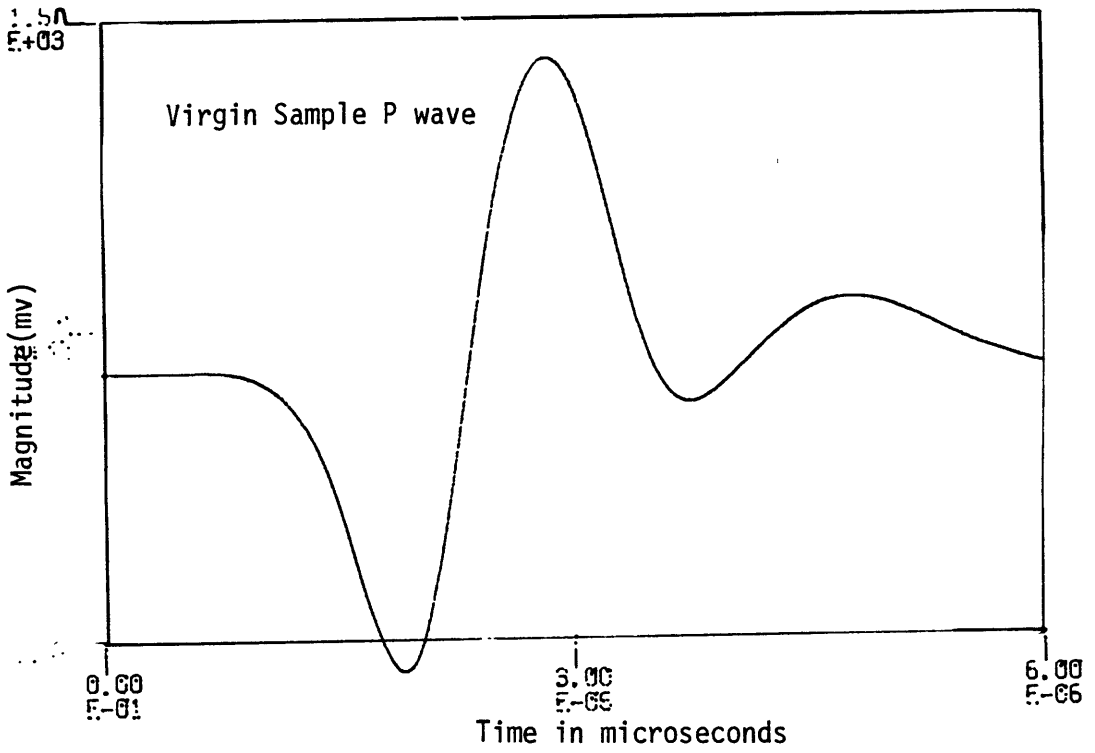
Virgin Sample P wave
Magnitude (mv)
0.00
E-01
3.00
E-06
6.00
E-06
Time in microseconds

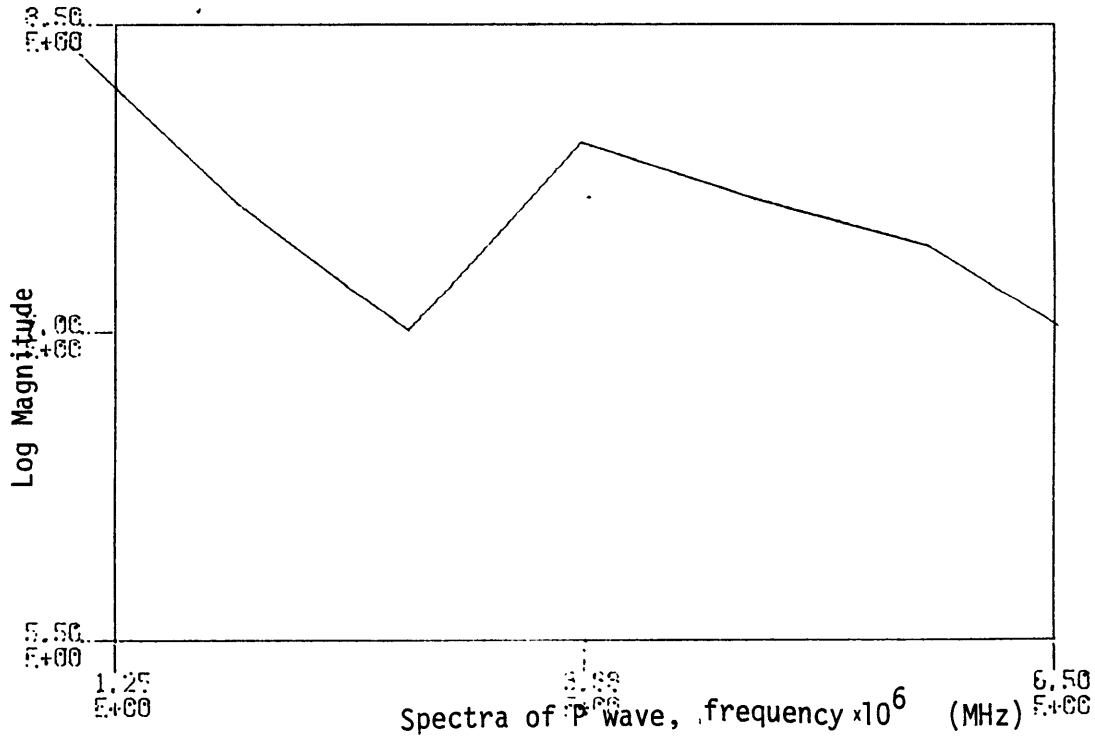
Log Magnitude
1.25
E+00
6.50
E+06
Spectra of P wave, frequency x10^6 (MHz)

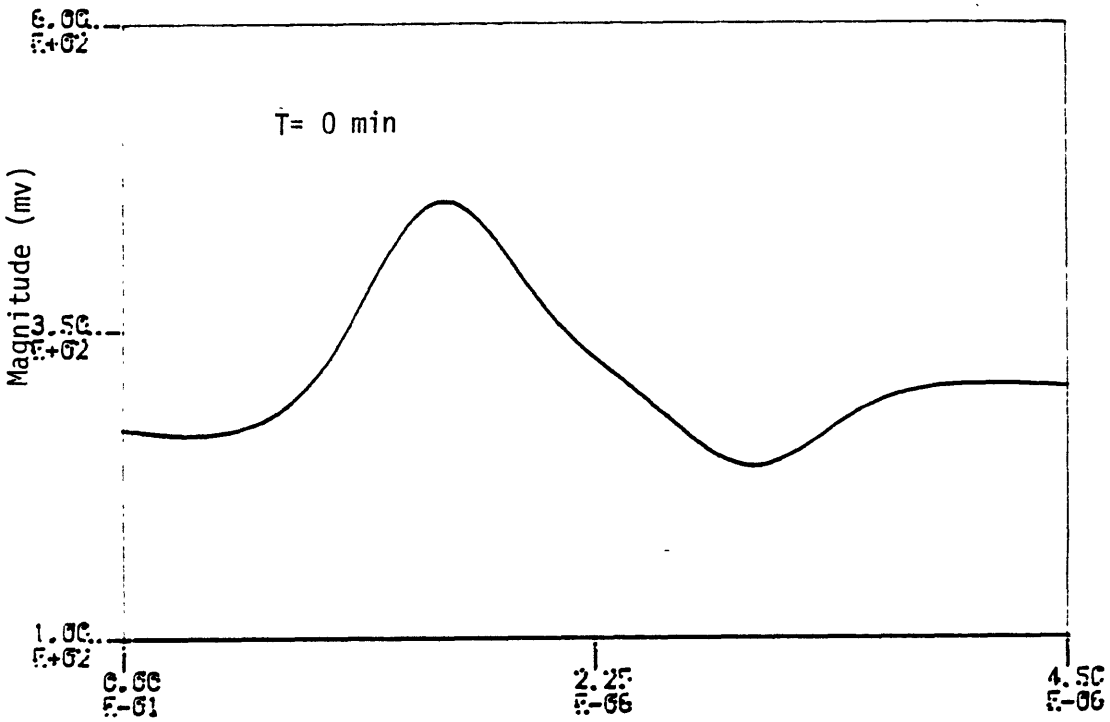

S wave cycle 1 time in microseconds

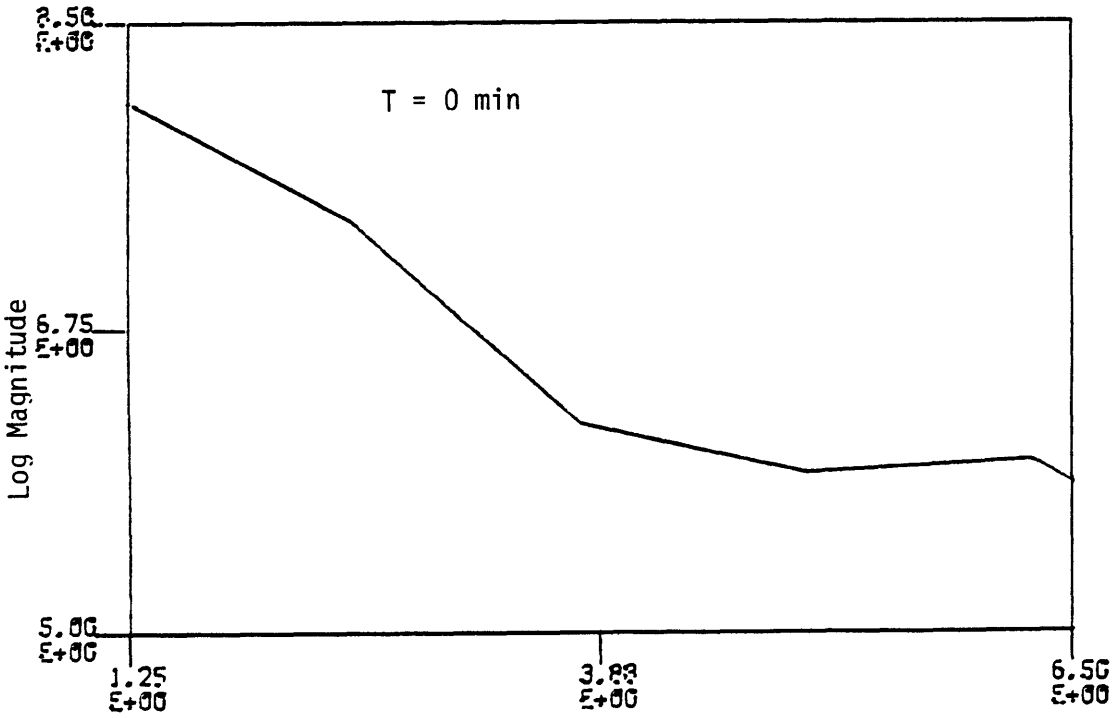

Spectrum of S wave, frequency $\times 10^6$

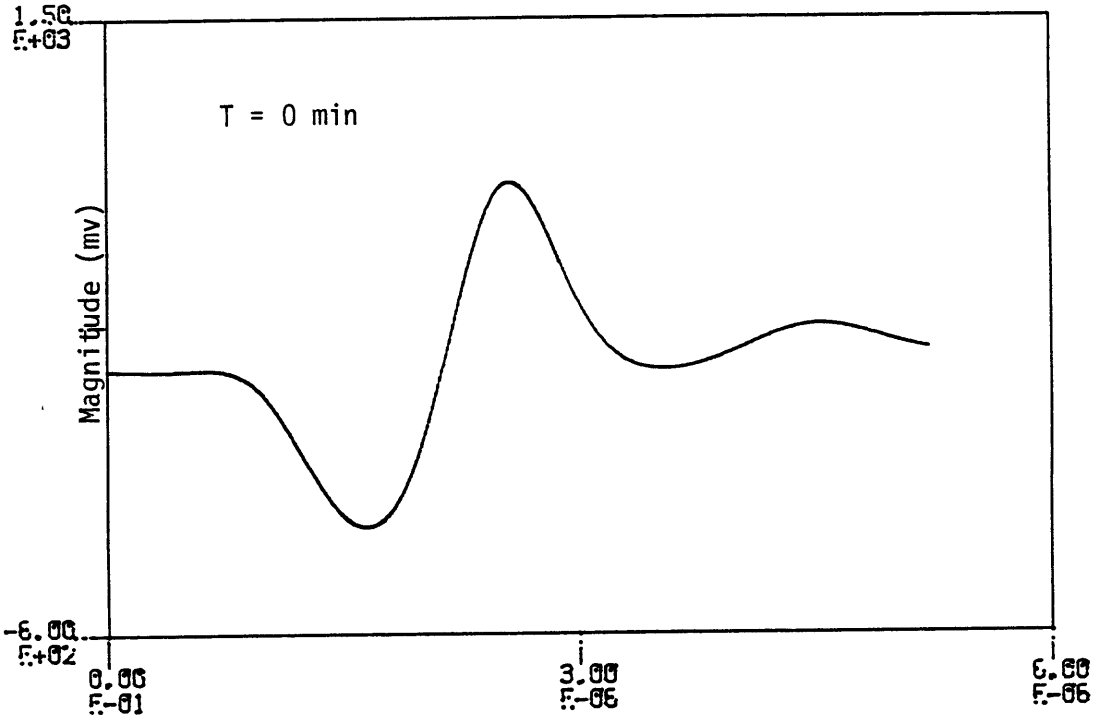

P wave, cycle 1, time in microseconds

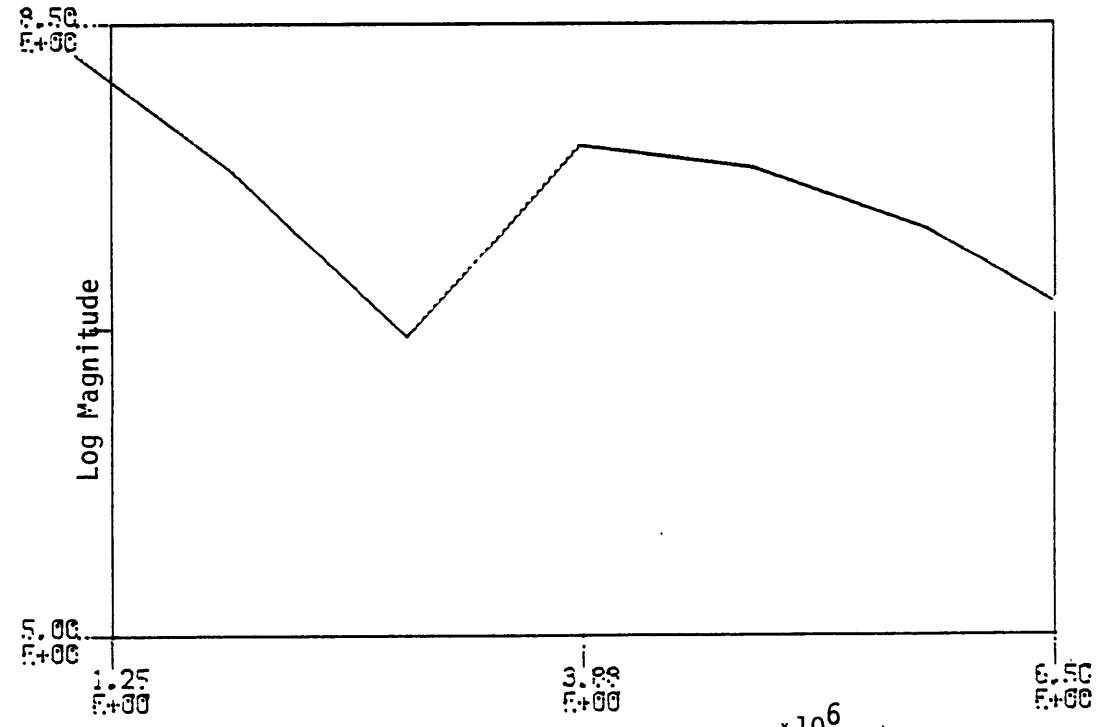

Spectrum of P wave, Frequency $\times 10^6$

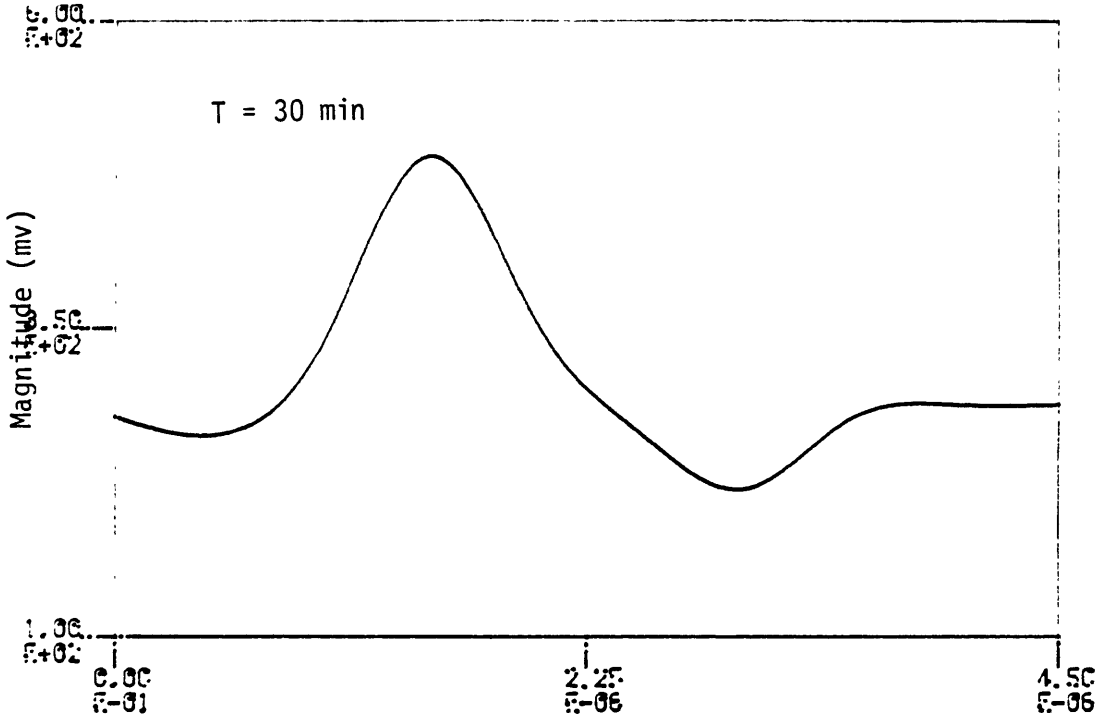

S wave, Cycle 1 , time in microseconds

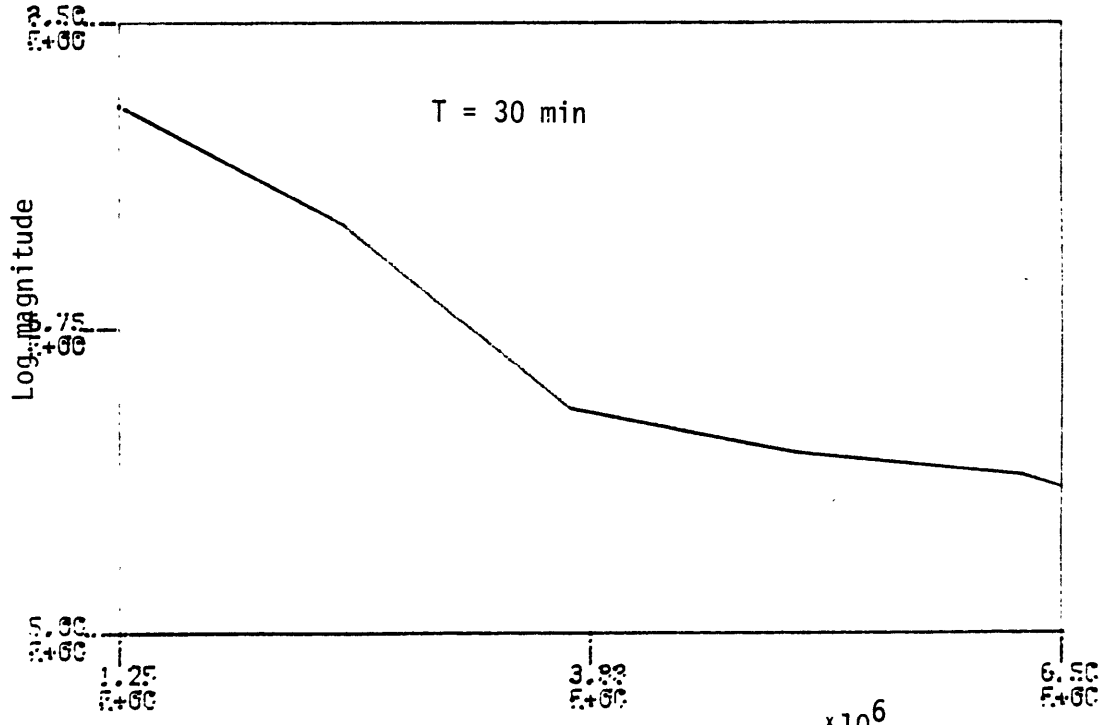

Spectrum of S wave, Frequency $\times 10^6$

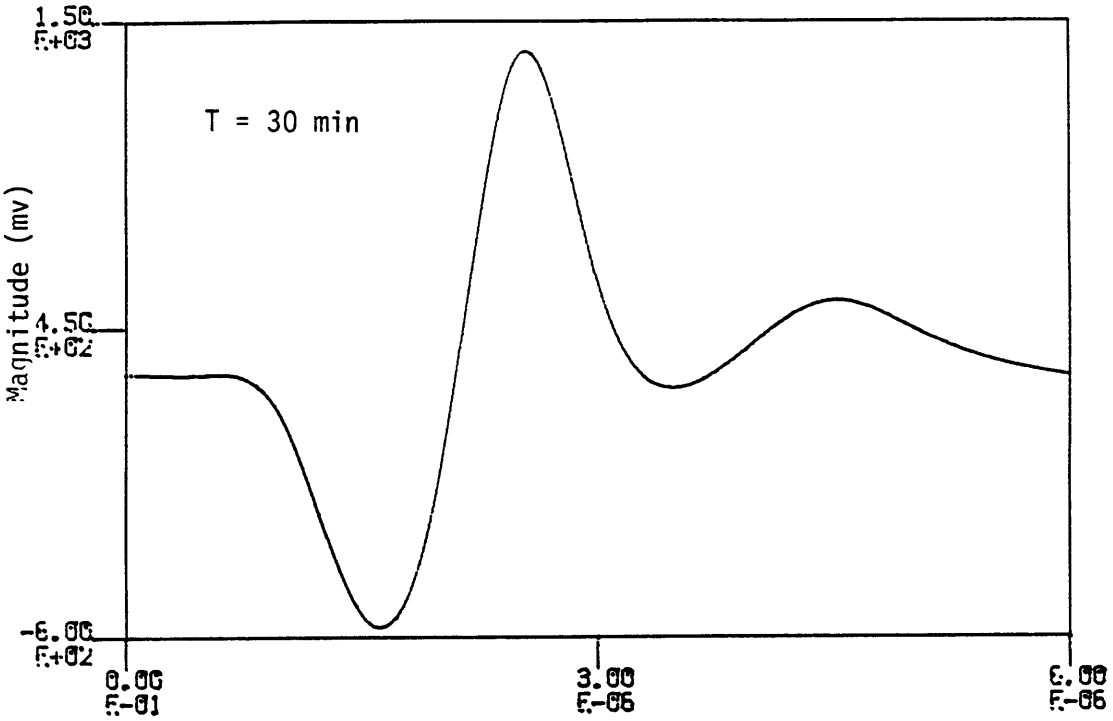

P wave, cycle 1, time in microseconds

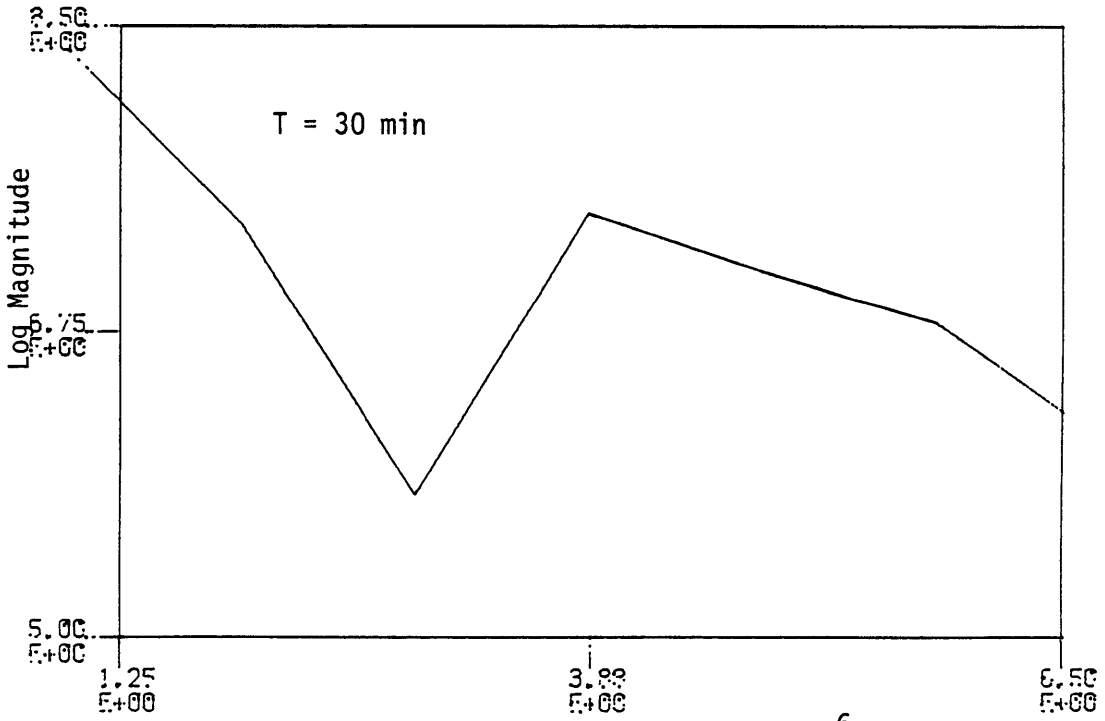

Spectrum of P wave, Frequency $\times 10^6$

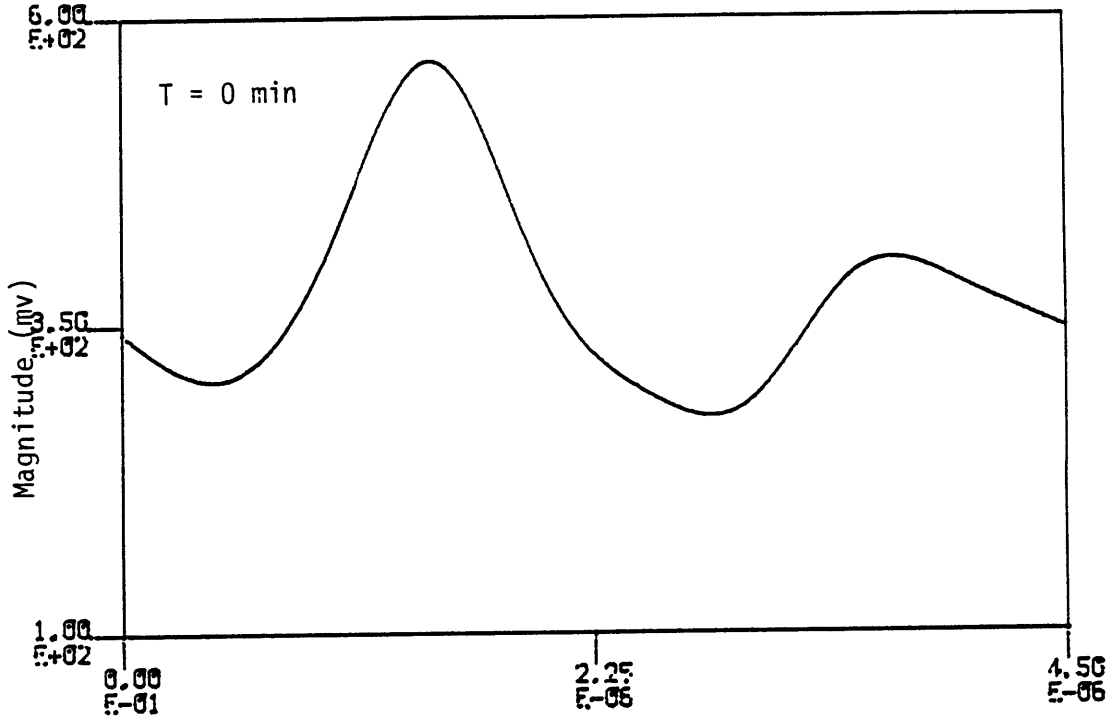

S wave , Cycle 2, time in microseconds

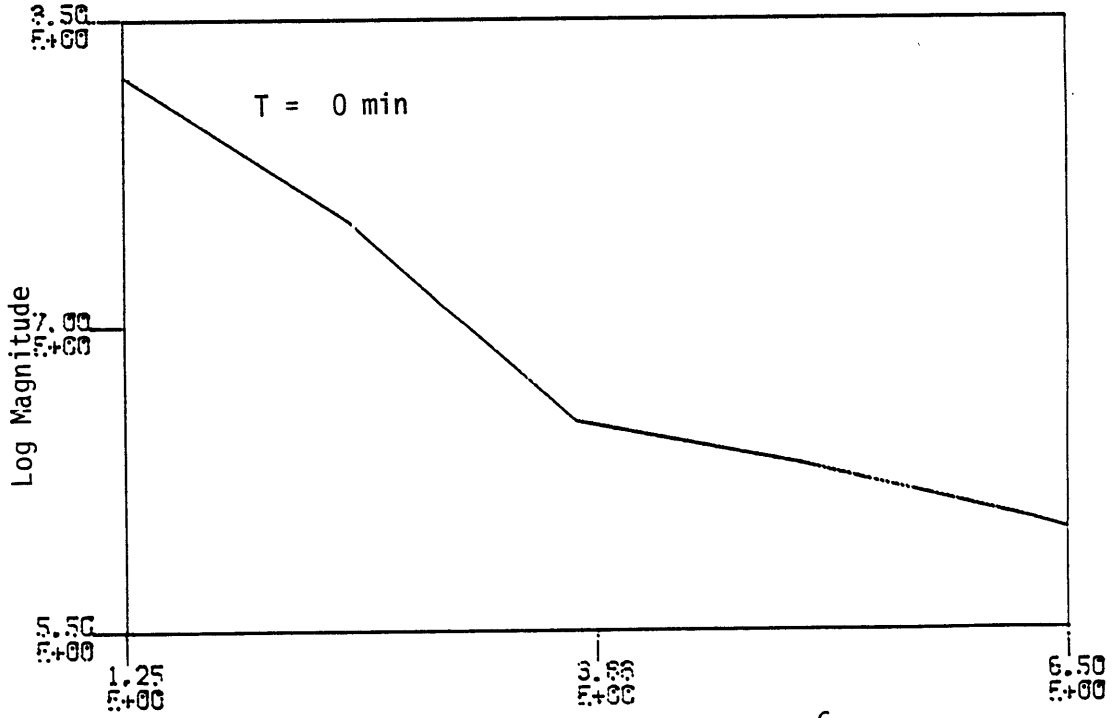

Spectrum of S wave, Frequency $x10^6$

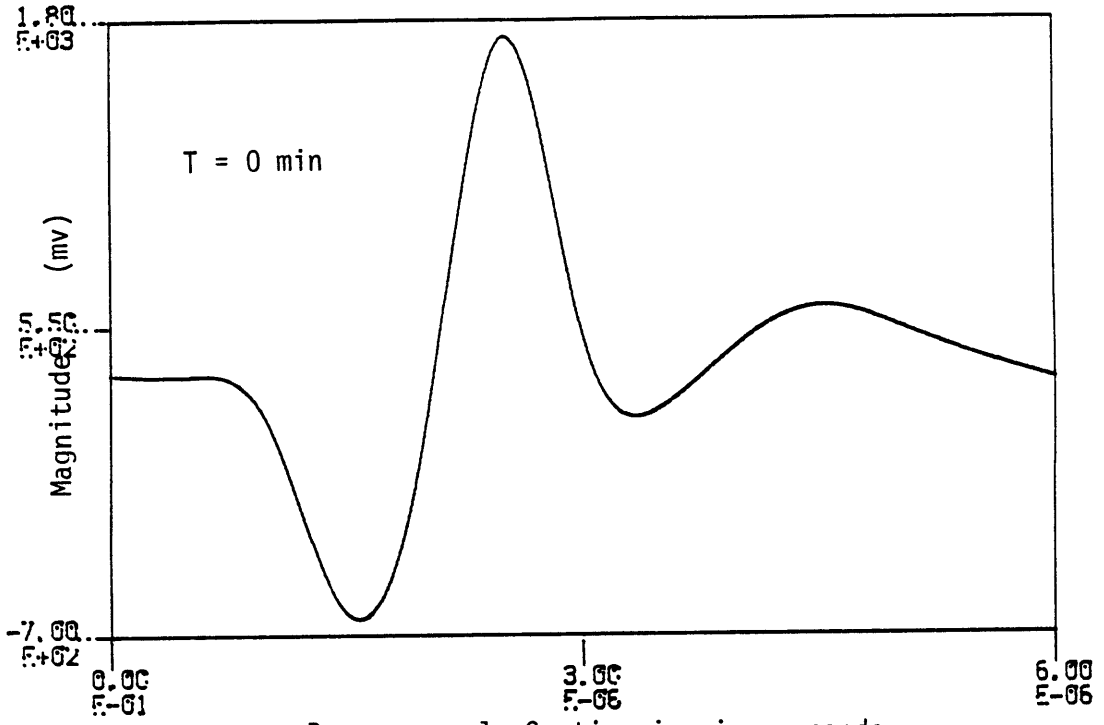

P wave, cycle 2, time in microseconds

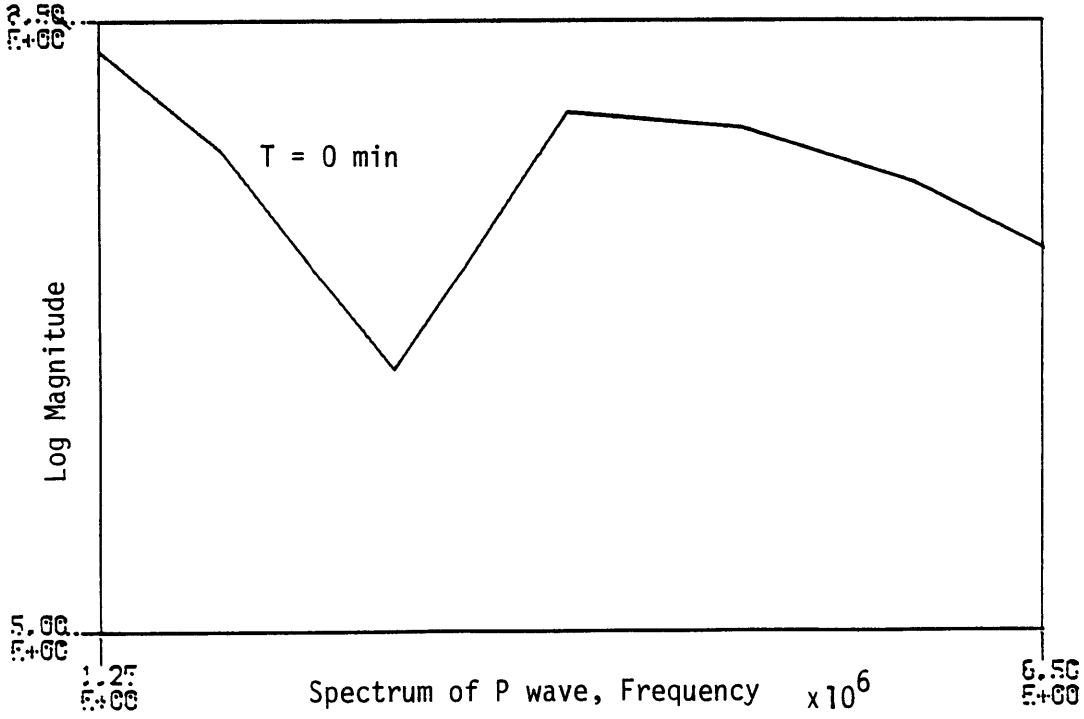

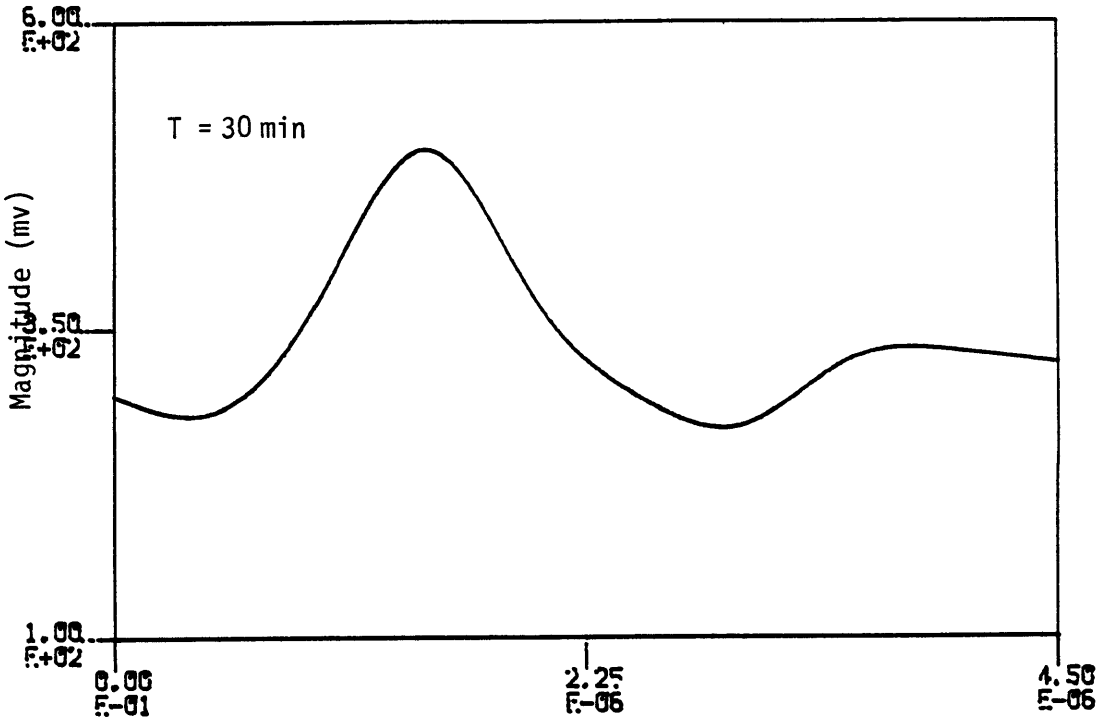

S wave, cycle 2, time in microseconds

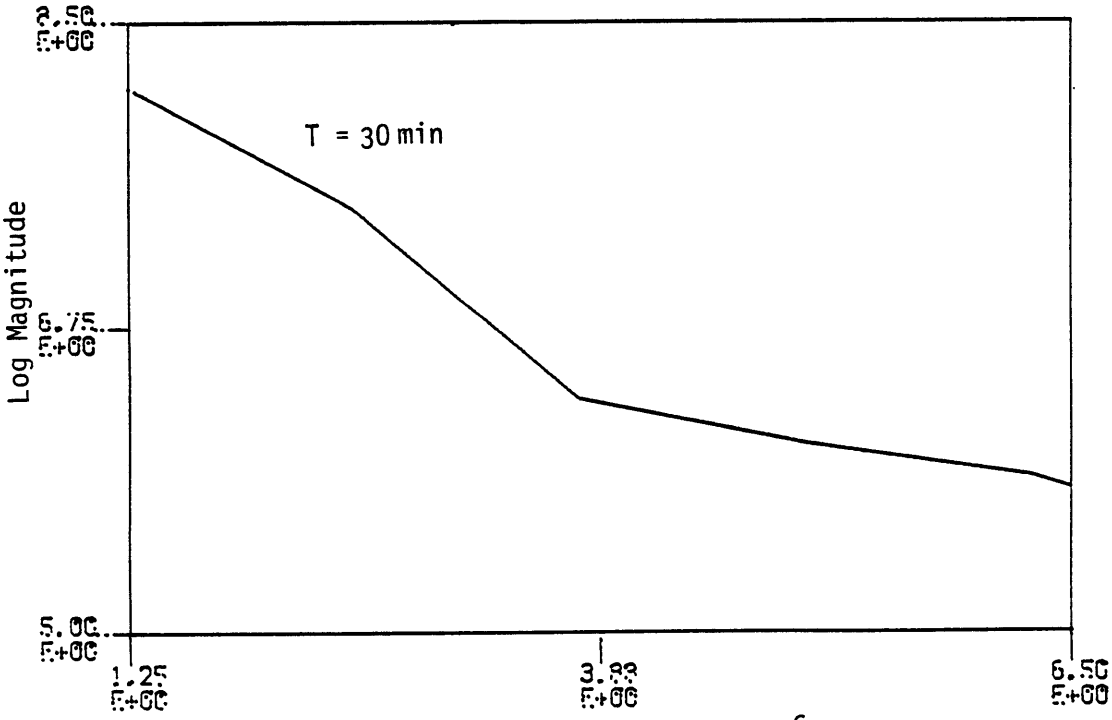

Spectrum of S wave, Frequency $\times 10^6$

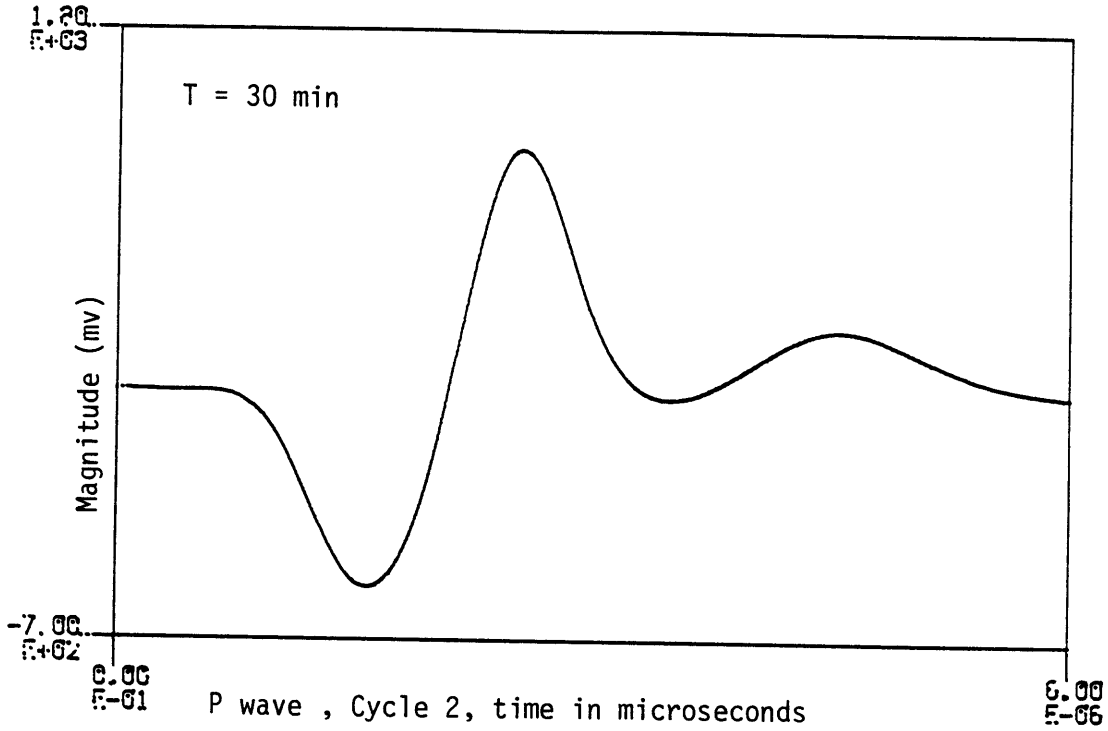

P wave , Cycle 2, time in microseconds

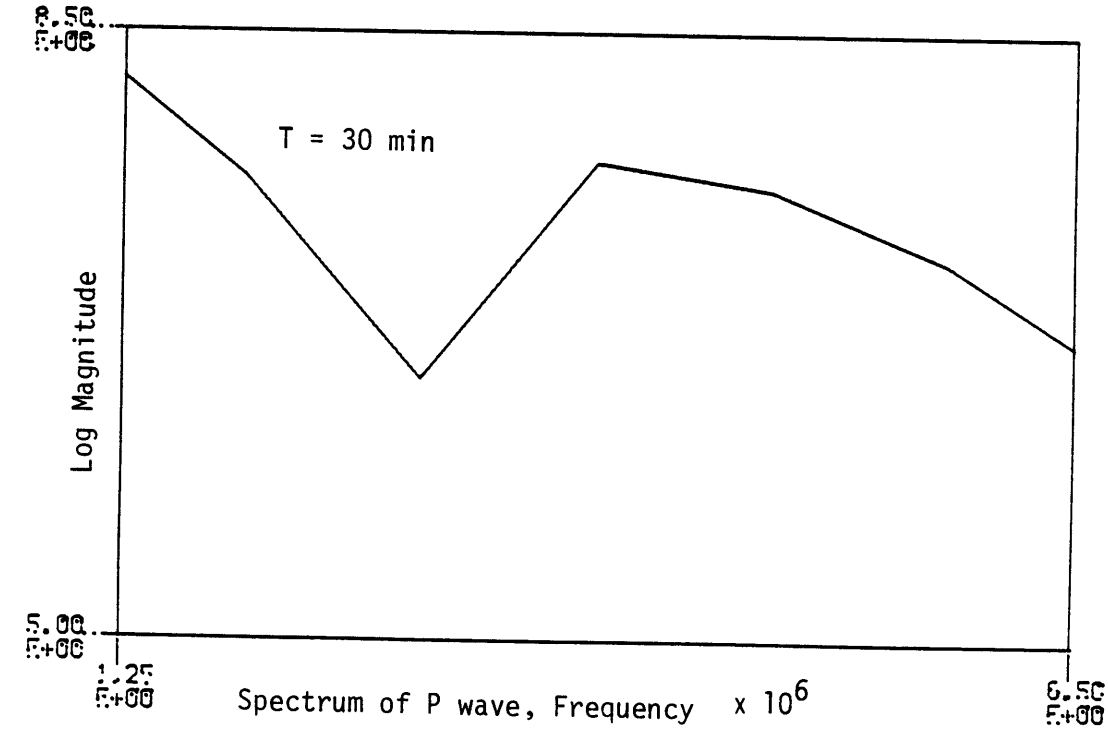

Spectrum of P wave, Frequency x 10^6

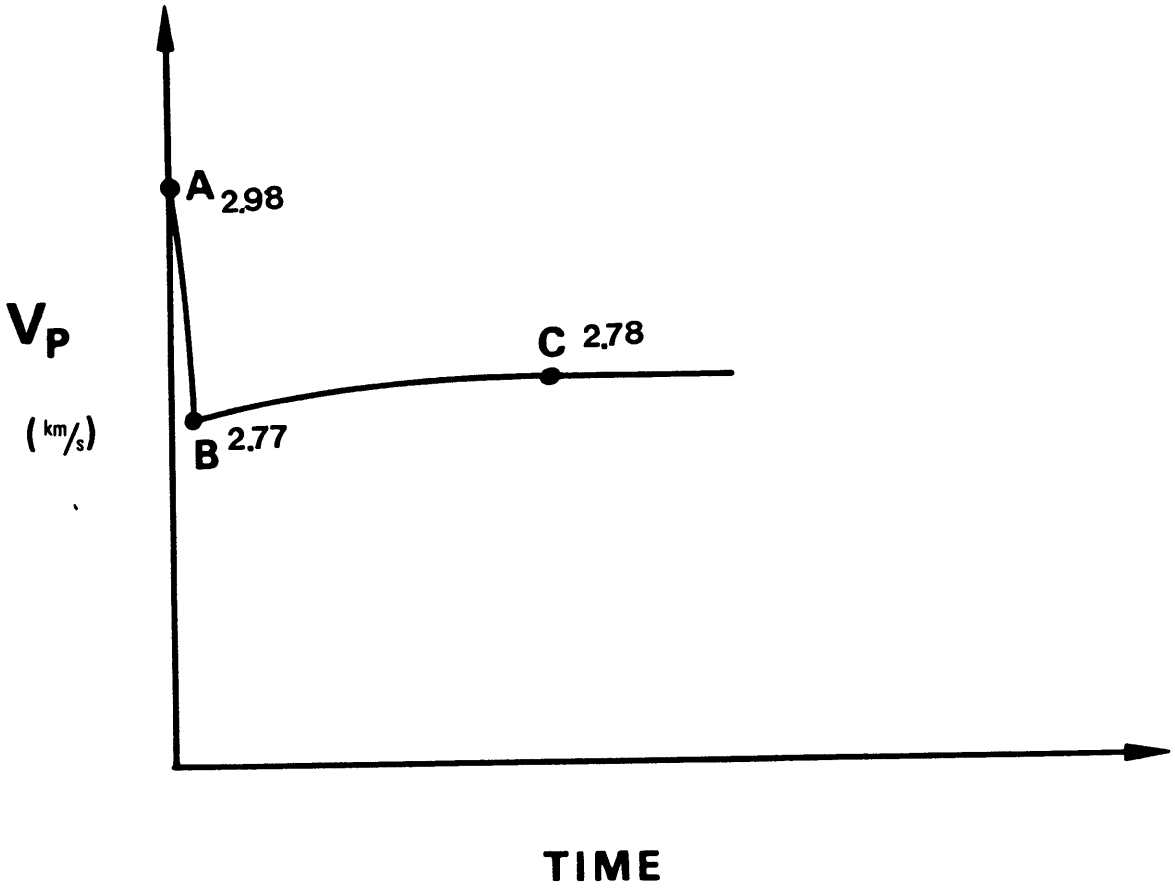

Figure 2: Typical velocity behavior as the confining pressure drops for a P wave. Values for drop from point A to B are typically in the range of 5 % of the steady state velocity C. Change in velocity from point B to C is as noted in the text less than 2%.

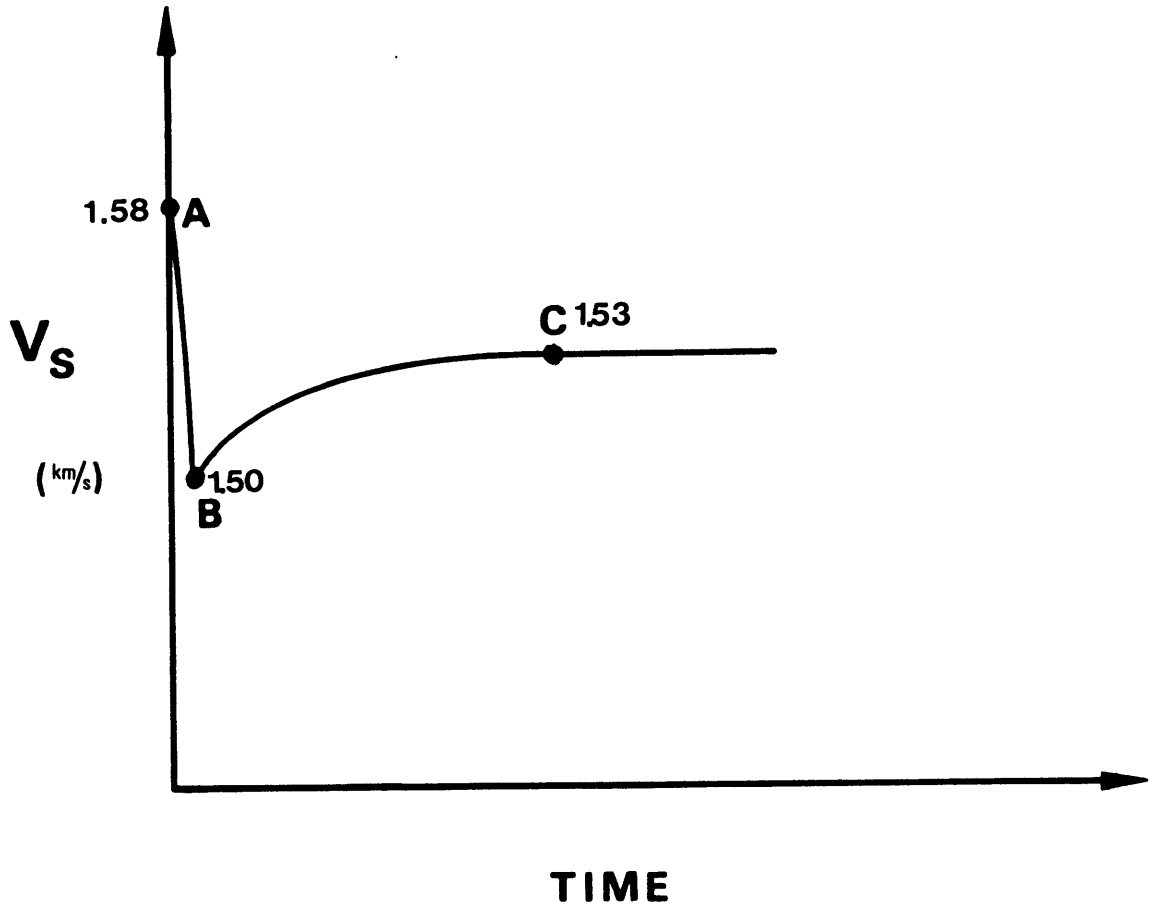

Figure 1: Typical velocity behavior as the confining pressure drops for an S wave. Values for drop from point A to B are typically in the range of 6-8% of the steady state velocity C. Change in velocity from point B to C is as noted in the text, approximately 3%.

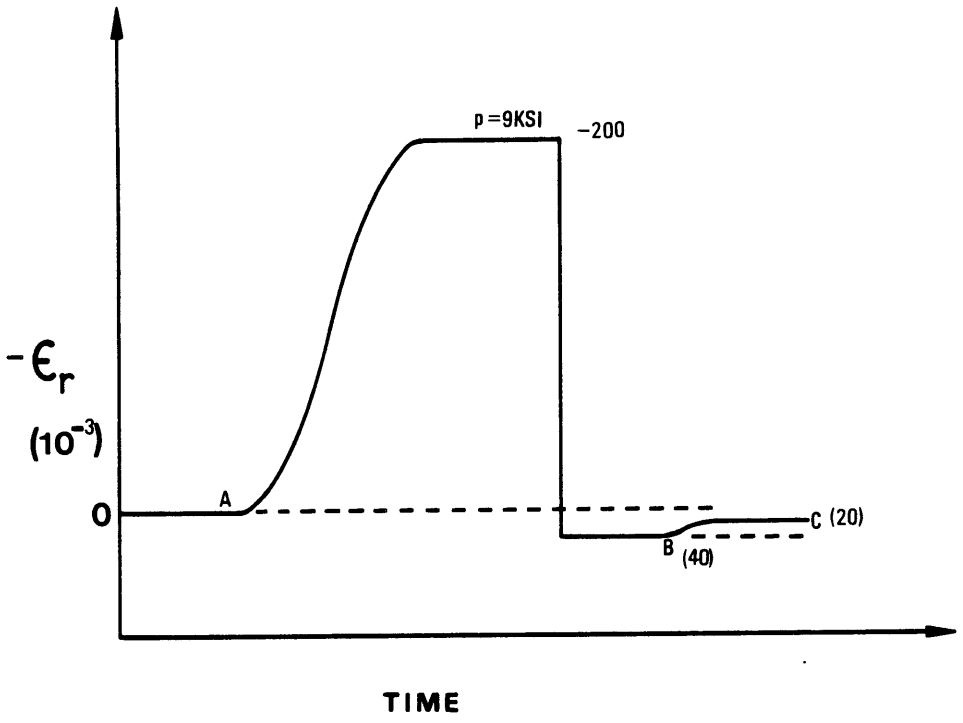

Figure 3: Radial strain behavior after pressure drop. Base values after pressure drop show sample to have slightly expanded, and decreasing in radius to a value slightly larger than the original.

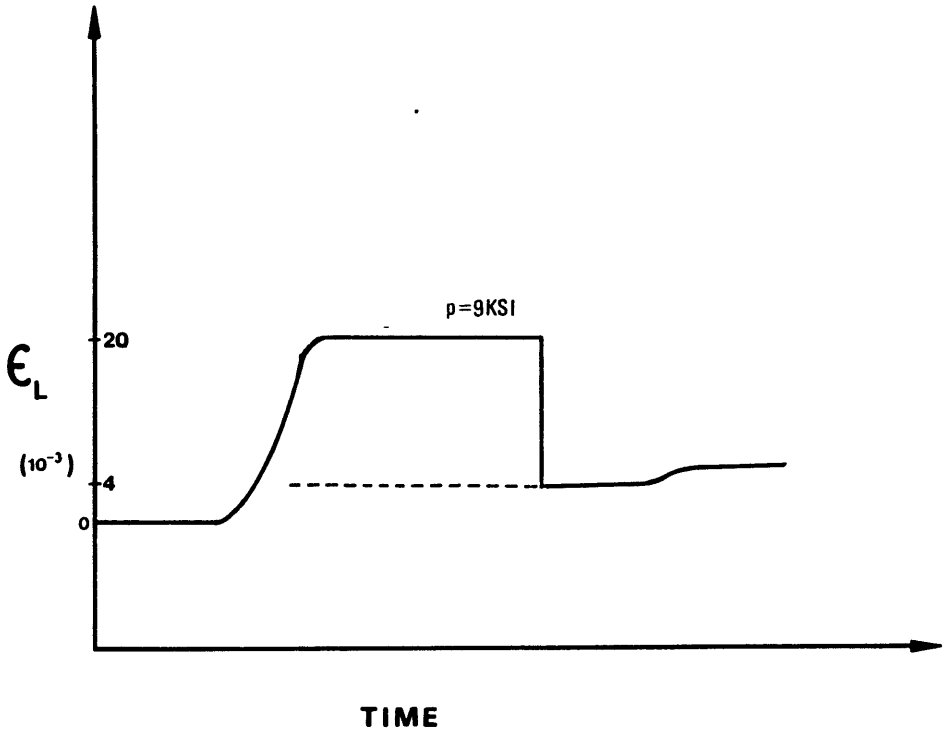

Figure 4: Axial Strain during entire pressure cycle

Values for Velocity Change Over Time

Saturated Samples	Shear	Compressiona
before pressure cycle:	1.62km/s	2.83km/s
after pressure cycle: (before pores equilibrate)	1.56km/s	2.77km/s
at steady state:	1.59km/s	2.78km/s

Appendix 2. The Determination of Velocity Data

The use of a wave propagation device in determining velocities and therefore the dynamic elastic properties is simple and straightforward process. The sample must be prepared with several specifications to insure accurate measurement of the acoustical properties.

- The sample must be representative of the whole rock mass, as well as homogeneous in structure itself.

- The length of the sample must be known at all times during the course of the experiment. The samples are measured to within half a thousandth of an inch and monitored by an LVDT during any deformation of the sample.

- Flatness is crucial to the use of the system. Surface grinders are preferred to acheive as smooth a surface as possible. Parallel sides are as important, and surface grinding is the accepted technique.

- Fluids can not be allowed between the sample and endcap due to their ability to attenuate the signal and/or cause erroneous travel times. A seal with a liquid urethane has adequately provided protection at the pressures acheived.

- Coupling of the sample to the endcaps must be a constant to the system over a number of runs . This accomplished by

    * Silver foil between the sample and endcap to smooth out any microscopic irregularities

    * Highly viscous fluid (Dow # 9) in an extremely thin layer to further provide the surfaces with improved contact

    * Placement of the sample is kept constant by the use of preloaded threaded rods holding the endcaps together (see figureELEC)

- Electronic settings should be as follows

* All equipment should be wired as shown in figure ELECT with insulated coaxial cable of 50 ohm impedence.

* The panametrics can be set for either single or double transducer operation. The user should be intimately familar with the operation of the pulser/receiver before use. No settings above 2 on the power level should be used with the present set of transducers. Other settings are for the particular sample characteristics and the user should become familar with the 5055 unit's range of capablities.

* The transducers should be attached to the switches as shown on the wires, and the signal can be routed through an optional band-pass filter if desired. Attachment to the digital scope should be in the lowest voltage selection for most samples. The time per point should be as high as possible. Arrivals for typical samples (approximately two inches) are usually less than 50 micro seconds.

$$G = \rho V_S^2 \tag{1}$$

$$K = \rho \, [V_P^2 - 4/3V_s^2] \tag{2}$$

$$E = 9KG \; / \; [3K + G] \tag{3}$$

$$\nu = .5 \, [R^2 - 2] \; / \; [R^2 - 1] \tag{4}$$

where: G = Shear Modulus
K = Bulk Modulus
E = Young's Modulus
ν = Poisson's Ratio
ρ = Bulk Density
V_P = Compressional (P-wave) Velocity
V_S = Shear (S-Wave) Velocity
R = Ratio (V_P / V_S)

Appendix 3. Fortran Routines for Elastic Constant Determination

```
      DIMENSION ICOMM(40)
      INTEGER*2 FILNAM(5)
01    CONTINUE
      REAL L,K,NU
      ICOUNT=1
      ITELL=0
      RHOF=0.86
      RHOS=1.98
25    CONTINUE
      WRITE(5,100) RHOF
      WRITE(5,110) RHOS
100   FORMAT(' ','THE VALUE OF RHO(FLUID) IS',1X,F10.6,1X,'GM/CC')
110   FORMAT(' ','THE VALUE OF RHO(SOLID) IS',1X,F10.6,1X,'GM/CC')
      TYPE*,'DO YOU WISH TO CHANGE RHO(FLUID) OR RHO(SOLID)?'
      TYPE*,'(1=YES,0=NO)'
      ACCEPT*,ITELL
      IF(ITELL.NE.1)GOTO500
      TYPE*,'ENTER THE NEW VALUE OF RHO(FLUID) (GRAMS/CC)'
      ACCEPT*,RHOF
      TYPE*,'ENTER THE NEW VALUE OF RHO(SOLID) (GRAMS/CC)'
      ACCEPT*,RHOS
      GOTO25
500   CONTINUE
      TYPE*,'WHAT IS THE VALUE OF L (length) (CENTIMETERS) ?'
      ACCEPT*,L
      TYPE*,'WHAT IS THE VALUE OF T(p) (MICROSECONDS) ?'
      ACCEPT*,TP
      TYPE*,'WHAT IS THE VALUE OF T(s) (MICROSECONDS) ?'
      ACCEPT*,TS
      TP=TP*0.000001
      TS=TS*0.000001
      PHI=0.15
      RHOB=RHOF*PHI+(1-PHI)*RHOS
      DELTP=4.0*0.000001
      DELTS=7.6*0.000001
      VP=(L/(TP-DELTP))
      VS=(L/(TS-DELTS))
      R=VP/VS
      G=(RHOB*VS**2)*.0000145
      K=(RHOB*(VP**2-(4*VS**2)/3))*.0000145
```

```
      E=9*K*G/(3*K+G)
      NU=0.5*((R**2)-2)/((R**2)-1)
      VPS=VP/100000.
      VSS=VS/100000.
      WRITE(5,200) VPS
      WRITE(5,210) VSS
      WRITE(5,215) G
      WRITE(5,220) E
      WRITE(5,225) K
      WRITE(5,230) NU
200   FORMAT(' ','THE VALUE OF V(p)=',1X,F9.4,1X,'KILOMETERS/SEC')
210   FORMAT(' ','THE VALUE OF V(s)=',1X,F9.4,1X,'KILOMETERS/SEC')
215   FORMAT(' ','THE VALUE OF G   =',1X,1PG15.7,1X,'PSI')
220   FORMAT(' ','THE VALUE OF E   =',1X,1PG15.7,1X,'PSI')
225   FORMAT(' ','THE VALUE OF K   =',1X,1PG15.7,1X,'PSI')
230   FORMAT(' ','THE VALUE OF NU  =',1X,F7.5,1X,'(DIMENSIONLESS)')
      TYPE*,'DO YOU WANT TO SAVE THIS DATA ON A FILE?'
      TYPE*,'(1=YES,0=NO)'
      ACCEPT*,IFILE
      IF(IFILE.NE.1)GOTO997
      TYPE*,'WHAT DO YOU WANT TO NAME THE FILE?'
      ACCEPT400,FILNAM
400   FORMAT(5A2)
      OPEN(UNIT=10,NAME=FILNAM,TYPE='NEW',FORM='FORMATTED')
      WRITE(10,200) VPS
      WRITE(10,210) VSS
      WRITE(10,215) G
      WRITE(10,220) E
      WRITE(10,225) K
      WRITE(10,230) NU
      TYPE*,'DO YOU WANT TO ENTER COMMENTS INTO THE FILE?'
      TYPE*,'(1=YES,0=NO)'
      ACCEPT*,ICOM
      IF(ICOM.NE.1)GOTO998
      TYPE*,'ENTER COMMENTS...'
      TYPE*,'ENTER A QUESTION MARK ( ? ) TO TERMINATE'
360   ACCEPT340,NCHRS,(ICOMM(I),I=1,NCHRS)
340   FORMAT(Q,40A2)
      WRITE(10,350) (ICOMM(I),I=1,NCHRS)
350   FORMAT(' ',40A2)
      IF(ICOMM(1).NE.'?')GOTO360
998   CLOSE(UNIT=10)
997   TYPE*,'DO YOU WANT TO RUN AGAIN? (1=YES,0=NO)'
      ACCEPT*,IRAG
      IF(IRAG.EQ.1)GOTO01
```

```
999     CONTINUE
        STOP
        END
```

appendix 4. Fortran Routines for Data Transfer

```
C  NICOLET DATA DUMP PROGRAM
C
C
C   FAST DATA DUMP FROM NICOLET PROGRAM USING BINARY OUTPUT.
C  NTN(I)=SCOPE DISK TRACK NUMBER(ENTERED BY USER)(I TH ENTRY)
C  MF7(I)=FILE SIZE OF TRACE #I
C  NTN(I)=ARRAY TO STORE NIC DISK TRACKS TO DUMP.
      BYTE BY(8192),MESS(27),MESSAG(2),HEAD(80)
      INTEGER*2 BYT(4096),NTN(8),MF1(4),MF7(8)
      INTEGER*4 T1,T2,TR              !TIMING VARIABLES
      EQUIVALENCE (BY,BYT)            !BINARY DATA IS TRANSLATED
      COMMON BY                       !TO INTEGER HERE.
      DATA MF1/4096,2048,2048,1024/
      DATA MESSAG(1)/"122/                !OCTAL 122="R"
      TYPE *,' NICOLET DUMP PROGRAM'
      TYPE *,' HOW MANY MEMORY TRACKS DO YOU WISH TO DUMP?'
      TYPE *,' (NOTE THAT ALL WILL END UP IN ONE FILE:FTN1.DAT)'
      TYPE *,' ENTER 1 TO 8 '
      ACCEPT 10,NT                !NT=NUMBER OF TRACKS
      IF(NT GT.1) GO TO 20
      NTN(1)=0                    !SELECTED THE CURRENT TRACE OPTION
      TYPE *,' ENTER MEMORY FRACTION OF CURRENT TRACE:(ALL=1,H=2,Q=4)'
      ACCEPT 10,MF7(1)
        TYPE *,' ENTER ALPHANUMERIC HEADER STRING (MAX 80 CHAR) '
        ACCEPT 977,HEAD
 977    FORMAT(80A1)
        WRITE(1,977) HEAD
      GO TO 64
  20  WRITE(5,50) NT          !ASK THE USER FOR TRACK #'S AND MF'S
      DO 60 I=1,NT
      WRITE(5,998) I          !ENTER TRACK NUMBERS
      ACCEPT 10,NTN(I)
      WRITE(5,999) NTN(I)     !ENTER MEMORY FRACTION FOR TRACK
      ACCEPT 10,MF7(I)
  60  CONTINUE
  64  CONTINUE
      DO 30 I=1,NT            !START MAIN LOOP
      DO 35 J=1,4096          !ZERO THE BYTE ARRAY OF PREVIOUS DATA
      BYT(J)=0                !BYT WILL CATCH THE INTEGER DATA.
  35  CONTINUE
```

```
      DO 36 J=1,27              !MESS IS THE BYTE ARRAY WITH THE
      MESS(J)=0                 !NORMALIZING DATA. ZERO IT.
   36 CONTINUE
      MF=MF7(I)
      MF6=NTN(I)
      ENCODE(1,10,MESSAG(2)) MF6  !MESSAG(1) HAS "R" IN IT.
      CALL IBDCL             !AN ENCODE STMT CONVERTS THE # IN MF6
      CALL IBIFC             !INTO AN ASCII CHARACTER IN MESSAG(2).
      IF(MF6 EQ.0) GO TO 300 !DON'T RECALL A TRACK IF YOU WANT THE
C  CURRENT MEMORY CONTENTS.
      CALL IBSEND(MESSAG,2,15)
C IBSEND SENDS THE ASCII CHARACTERS IN MESSAG DOWN THE IEEE BUS TO
C ADDRESS 15.  15 IS THE NICOLET COMMAND CENTER.
  300 CONTINUE
      CALL IBDCL                !RESETS DEVICES ON THE IEEE BUS TO
C  DEFAULT CONDITION
      CALL GTIM(T1)           !FIND OUT WHAT TIME IT IS TO TIME RUN.
      CALL IBTERM
C!THIS INSTRUCTS MINC TO ACCEPT A
C CARRIAGE RETURN ONLY AS A MESSAGE TERMINATOR ON THE IEEE BUS.
C THIS TURNED OUT TO BE NECESSARY FOR MY SUBROUTINE NIC SINCE
C IBRECV IS CALLED ONLY ONCE AND ACCEPTS SEVERAL CHARACTERS AS A
C TERMINATOR.  WE WERE ONLY GETTING PART OF THE DATA ACROSS THE BUS
C
C NIC HANDLES RECEIVING THE NORMALIZING AND INTEGER DATA AND IS A
C GENERAL PURPOSE SUBROUTINE. MF=MEMORY FRACTION OF TRACE IN SCOPE
C MEMORY(ACCORDING TO THE USER)  MESS=NORMALIZATION DATA
C  JN=NUMBER OF BYTES OF DATA RECEIVED ON FIRST TRY. 1-DATA POINT
C =2 BYTES   IFLAG= NUMBER OF DATA POINTS CAUGHT ON SECOND TRY.
C IFLAG SHOULD BE =0 UNLESS SOMETHING ISN'T RIGHT.
      CALL NIC(MF,MESS,IFLAG,JN)
      CALL GTIM(T2)                          !FIND OUT WHAT TIME IT IS
      CALL JSUB(T2,T1,TR)                    !SUBTRACT TIME1 FROM TIME2
      CALL CVTTIM(TR,IH,IM,IS,IT)
C CONVERT TIME TO HOURS,MINUTES,SECONDS AND TICKS.(1 TICK= 1/60TH OF
C A SECOND).
      IF(IFLAG.NE.0) WRITE(5,395) JN,IFLAG
C LET USER KNOW DATA DUMP DIDN'T GO SMOOTHLY.
      WRITE(5,90)IH,IM,IS,IT                 !TELL HOW LONG IT TOOK
      MF2=MF1(MF)                            !MF2 IS HOW MANY DATA POINTS
C THERE SHOULD BE IN THIS TYPE OF FILE.
C
C HERE FRDNIC DECODES THE HEADER DATA TO PRODUCE NORMALIZATION DATA
C IN INTEGER FORMAT.
      DECODE(5,120,MESS(4)) IV0              !LOCATION OF ZERO VOLTAGE
```

```
C WITH RESPECT TO NICOLET SCREEN ZERO.
      DECODE(5,120,MESS(9)) IH0              !TIME ZERO LOCATION
      DECODE(1,10,MESS(14)) MXVN             !MANTISSA OF VOLTAGE NORM
      DECODE(3,130,MESS(18)) IEXVN           !EXPONENT OF VOLTAGE NORM
      DECODE(1,10,MESS(21)) MXHN             !MANTISSA OF TIME NORM
      DECODE(3,130,MESS(25)) IEXHN           !EXPONENT OF TIME NORM
      XVN=MXVN*10.**IEXVN                !REPRODUCE INTEGER NORM MULTIPLIERS
      XHN=MXHN*10.**IEXHN
      XV0=-1*IV0*XVN                     !PUT VOLTAGE AND TIME ZERO DATA IN
      XH0=-1*IH0*XHN                     !THE FORMAT OF DC-OFFSETS.
      XNP=4096/MF                        !CONVERT MF TO #OF DATA DUMPED.
      WRITE(1,140) XV0,XH0,XVN,XHN,XNP   !WRITE NORM TO FTN1.DAT
      DO 31 J=1,MF2,4
      WRITE(1,110) BYT(J),BYT(J+1),BYT(J+2),BYT(J+3),J !WRITE DATA
   31 CONTINUE
   30 CONTINUE                   !LOOP BACK FOR OTHER SCOPE TRACKS.
      CALL IBDCL
      TYPE *,' PROGRAM COMPLETE'
   10 FORMAT(I1)
   50 FORMAT(2X,' ENTER NAMES OFTHE ',I1,' TRACKS YOU WISH TO DUMP.',
     1/,' AND THE MEMORY FRACTION OF THAT TRACK.',
     2/,' NOTE.ENTER A "0" IF YOU WISH THE TRACK CURRENTLY IN MEMORY.',
     3//,' ENTER TRACK #:')
   90 FORMAT(' ',I2,'HOURS',3X,I2,'MINS',3X,I2,'SECS+',I2,'1/60THS')
  110 FORMAT(4I5,10X,I5)
  120 FORMAT(I5)
  130 FORMAT(I3)
  140 FORMAT(5E15.6)
  395 FORMAT(' ONLY READ:',I5,'POINTS THE FIRST TIME AND',I5,
     1' POINTS THE SECOND TRY.')
  415 FORMAT(2I1)
  998 FORMAT(' ENTER THE',I1,'TH TRACK NUMBER:')
  999 FORMAT(' ENTER THE MEMORY FRACTION OF TRACK #',I1,
     1/,' MEMORY FRACTION=(ALL=1,H=2,Q=4):')
      STOP
      END
      SUBROUTINE NIC(MF,MESS,IFLAG,JN)
C  PROGRAM NIC
C  FAST ROUTINE TO GET DATA OUTPUT FROM NICOLET.
C
C  INPUT-  MF = MEMORY FUNCTION 4-Q ; 2-H ; 1-A INTEGER.
C OUTPUT-  BY = BINARY ARRAY.DIMENSION:MF=4:1024,MF=2:2048,MF=1:4096
C OUTPUT-MESS = BYTE ARRAY=NORM DATA IN ASCII. (27 IN LENGTH)
C OUTPUT-IFLAG=0 IF DUMP WENT SMOOTHLY,OR #OF DATA POINTS IF IT DIDN'T
C OUTPUT-JN   = NUMBER OF DATA POINTS DUMPED ON FIRST TRY.
```

```
C NOTE THAT DATA GETS PASSED TO THE MAIN PROGRAM BY THE COMMON BLOCK BY
      BYTE BYT,BY(8192),MEM(7),MESS(27)
      INTEGER*2 CNT(7)
      COMMON BY
      DATA MEM/'0','1','2','3','4','5','6'/     !USED BELOW TO DECODE
C "STATUS BYTE" DATA RECEIVED FROM NICOLET. SEE PAGE X-10 IN THE
C "2081 ACESSORY" SECTION OF THE NICOLET OPERATION MANUAL.
      DATA CNT/1024,1024,1024,1024,2048,2048,4096/  !THIS IS THE ARRAY
C WHICH USES THE MEMORY SWITCH POSITION TO TELL YOU HOW BIG THE
C MEMORY IS THAT THIS TRACE IS STORED IN.
      IFLAG=0                                   !SET DEFAULT ERROR FLAG
      CALL IBSEND('D4',2,15)                    !ASK FOR "D4" OUTPUT
C MESS RECEIVES TWO ASCII NUMBERS: THE TRACK NUMBER THAT THE NICOLET
C DISK IS SET TO, AND THE MEMORY SWITCH POSITION.
      IST=IBRECV(MESS,2,14)
      DO 101 I=1,7
      IF(MESS(2) NE.MEM(I)) GO TO 101     !FIND OUT THE ACTUAL MEMORY
C SWITCH POSITION FROM THE "D4" OUTPUT.
      IC=CNT(I)                        !IC=NUMBER OF DATA POINTS IN MEMORY
      ICB=IC*2                         !ICB=CORRESPONDING NUMBER OF BYTES
      IF(I LE.4.AND.MF.EQ.4) GO TO 1
      IF(I LE.6.AND.I.GE.5.AND.MF.EQ.2) GO TO 1
      IF(I EQ.7.AND.MF.EQ.1) GO TO 1
      GO TO 2
 101  CONTINUE
  2   TYPE *,' MEMORY SWITCH ERROR-SETTING .NE. GIVEN VALUE'
C IF THE USER FIBBED ON THE MEMORY SWITCH POSITION, BOMB OUT
      STOP
  1   CALL IBSEND('D2',2,15)          !TELL NIC TO DUMP BINARY DATA
      JN=IBRECV(BY,ICB,14)            !CATCH IT IN "BY". JN=#BYTES
      JN1=ICB-10
      IF(JN.GE JN1) GO TO 450         !IF GOT MOST OF IT GO ON.
      JN2=ICB-1-JN
      JN3=JN+2
      JN4=IBRECV(BY(JN3),JN2,14)      !OTHERWISE TRY ONCE MORE
      IFLAG=JN4+JN
C THE NEXT SECTION OF CODE IS NECESSARY BECAUSE DIGITAL STORES THE LOW
C ORDER BYTE FIRST WHILE NICOLET SENDS THE HIGH BYTE FIRST.
 450  DO 100 I=1,ICB,2
      BYT=BY(I)
      I1=I+1
      BY(I)=BY(I1)
 100  BY(I1)=BYT
      CALL IBSEND('N1',2,15)          !TELL NIC TO SEND NORMALIZATION DATA
      IST=IBRECV(MESS,27,14)          !CATCH IT IN MESS.
```

```
CALL IBDCL                    !RESET NICOLET TO DEFAULT CONDITION.
RETURN                        !BYE
END
```

Appendix 5. Fast Fourier Transform Routine

```
      COMMON FR(1024),FI(1024)
      integer*2 filnam(5),foutmg(5),foutph(5)
      BYTE HEAD(10),XLBL(10),XMAGN(10),XREAL(10),XIMAG(10)
     1  ,XPHAS(10),XFREQ(10),XTIME(10)
      OPEN(UNIT=15,TYPE='OLD',FORM='FORMATTED')
      REWIND 15
      READ(15,700) XTIME
      READ(15,700) XREAL
      READ(15,700) XIMAG
      READ(15,700) XMAGN
      READ(15,700) XPHAS
      READ(15,700) XFREQ
      CLOSE(UNIT=15)
700   FORMAT(10A1)
      REAL MAG
      TTOTAL=100.
      VMAX=250.
      VMIN=-250
      YMAX=300.
      YMIN=-300.
      XMIN=0.
      XMAX=500.
      NPTS=1024
      MODE=1
      NTOT=1
      ILOST=0
      TIME=0.
      IAGIN=0
      ICON=1
      ISTOP=5
01    continue
      n=4096
      nl=0
      nlf=0
      type*,'FAST FOURIER TRANSFORM'
      do 40 i=1,1024
              fr(i)=0
              fi(i)=0
40    continue
      TYPE*,' '
```

```
      type*,'SPECIFY INPUT FILE NAME'
      accept400,filnam
400   format(5A2)
      open(unit=10,name=filnam,TYPE='OLD',FORM='UNFORMATTED') --
      rewind 10
      READ(10) NTOT
      TYPE*,' '
      TYPE*,'THE TOTAL NUMBER OF'
      TYPE*,' POINTS IN THE FILE = ',NTOT
      TYPE*,' '
      READ(10) (FR(I),I=1,NTOT)
      READ(10) IDUM
      IF(IDUM.NE.1)GOTO760
      READ(10) NTOT
      READ(10) (FI(I),I=1,NTOT)
      DO 765 I=1,NTOT
             FI(I)=0.
765   CONTINUE
760   CONTINUE
      READ(10) XHO
      READ(10) SAMINT
      READ(10) HEAD
      TYPE*,'THE SAMPLING INTERVAL OF'
      TYPE*,'THE POINTS = ',SAMINT
      TYPE*,' '
      TTOTAL=FLOAT(NTOT)*SAMINT*1000000.
      TYPE*,'THE POINTS WERE TAKEN OVER A TOTAL'
      WRITE(5,515) TTOTAL
515   FORMAT(' ','TIME PERIOD OF',/,F12.3,1X,'MICROSECONDS')
      TYPE*,' '
      CLOSE(UNIT=10)
505   FORMAT(I4)
510   FORMAT(F14.8)
      TYPE*,'ENTER STARTING POINT OF'
      TYPE*,'EVALUATION (MICROSECONDS)'
      ACCEPT*,STAR
      RSTAR=(STAR/1000000.)+SAMINT
      TYPE*,' '
      TYPE*,'ENTER NUMBER OF POINTS TO'
      TYPE*,'BE EVALUATED'
      ACCEPT*,NL
      FINAL=((FLOAT(NL)*SAMINT)*1000000.)+STAR
      RFINAL=(FLOAT(NL)*SAMINT)
      TYPE*,' '
      TYPE*,'THE FINAL POINT OF EVALUATION'
```

```
      TYPE*,'(MICROSECONDS) IS ',FINAL
      ISTART=IFIX(RSTAR/SAMINT)
      IFINAL=IFIX(RFINAL/SAMINT)
      TYPE*,' '
      TYPE*,'ENTER "M" (NUMBER OF OUTPUT POINTS)'
      TYPE*,'(MUST BE A POWER OF 2)'
      ACCEPT*,N
      TYPE*,' '
      NFILE=N/2+1
      type*,'OUTPUT AS'
      type*,'1)REAL AND IMAG.'
      TYPE*,'2)MAGN. AND FREQ.'
      TYPE*,'3)PHASE ANGLE'
      TYPE*,'4)ALL THREE'
      accept*,nout
      if(nout.EQ.1)goto705
      IF(NOUT.EQ.4)GOTO705
      GO TO 26
705   CONTINUE
      TYPE*,' '
      type*,'SPECIFY OUTPUT FILE NAME'
      TYPE*,'FOR REAL AND IMAGINARY PART DATA'
      accept430,filnam
430   format(5A2)
      TYPE*,' '
26    CONTINUE
      if(nout.EQ.2)goto710
      IF(NOUT.EQ.4)GOTO710
      GO TO 27
710   CONTINUE
      type*,'SPECIFY OUTPUT FILE NAME'
      TYPE*,'FOR MAGNITUDE AND FREQUENCY'
      accept450,foutmg
450   format(5A2)
      TYPE*,' '
27    CONTINUE
      IF(NOUT.EQ 3)GOTO715
      IF(NOUT.EQ.4)GOTO715
      GO TO 28
715   CONTINUE
      type*,'SPECIFY OUTPUT FILE NAME'
      TYPE*,'FOR PHASE ANGLE'
      accept460,foutph
460   format(5A2)
      TYPE*,' '
```

```
28      continue
        type*,'READING DATA'
        J=1
        DO 530 I=ISTART,IFINAL
                FR(J)=FR(I)
                J=J+1
530     CONTINUE
        TYPE*,' '
        type*,'CALCULATING FFT...'
        TYPE*,' '
C
C
C
550     call subfft(n)
C
C
        if(nout.eq.1)goto720
        IF(NOUT.EQ.4)GOTO720
        GO TO 200
720     CONTINUE
        open(unit=17,name=filnam,TYPE='NEW',FORM='UNFORMATTED')
        TYPE*,'WRITING REAL AND'
        TYPE*,' IMAGINARY PARTS...'
        TYPE*,' '
611     FORMAT(' ','REAL PART')
612     FORMAT(' ','IMAG PART')
        WRITE(17) N
        write(17) (fr(i),i=1,N)
        WRITE(17) ICON
        WRITE(17) N
        write(17) (fi(i),i=1,N)
        WRITE(17) XHO
        WRITE(17) SAMINT
        WRITE(17) XREAL
        WRITE(17) XIMAG
        WRITE(17) ISTOP
610     FORMAT(I4)
615     FORMAT(F14.8)
        close(unit=17)
200     CONTINUE
        if(nout.EQ.2)goto730
        IF(NOUT EQ.3)GOTO730
        IF(NOUT EQ.4)GOTO730
        GOTO997
730     CONTINUE
```

```
        type*,'CALCULATING MAGNITUDE, FREQUENCY'
        IF(NOUT.EQ.3)GOTO735
        IF(NOUT.EQ.4)GOTO735
        GO TO 736
735     CONTINUE
        TYPE*,'AND PHASE ANGLE...'
736     CONTINUE
        TYPE*,' '
        pi=3.141592654
        do 210 i=1,NFILE
                mag=SQRT(((ABS(fr(i)))**2)+((ABS(fi(i)))**2))
                if(mag.ne.0)goto220
                        ang=0
                        goto85
220             if(fr(i).eq.0)goto82
                if(fr(i).gt.0)goto230
                if(fi(i).lt.0)goto240
                goto250
230             ang=atan(fi(i)/fr(i))
                goto85
240             ang=atan(fi(i)/fr(i))-pi
                goto85
250             ang=atan(fi(i)/fr(i))+pi
                goto85
82              if(fi(i).le.0)goto260
                        ang=pi/2
                        goto85
260             ang=-pi/2
85              FR(I)=MAG
                fi(i)=ang
210             continue
        open(unit=15,name=foutmg,TYPE='NEW',FORM='UNFORMATTED')
        type*,'WRITING MAGNITUDE, FREQUENCY'
        IF(NOUT.EQ.3)GOTO740
        IF(NOUT EQ.4)GOTO740
        GO TO 741
740     CONTINUE
        OPEN(UNIT=16,NAME=FOUTPH,TYPE='NEW',FORM='UNFORMATTED')
        TYPE*,'AND PHASE ANGLE...'
        WRITE(16) NFILE
        WRITE(16) (FI(I),I=1,NFILE)
        WRITE(16) ISTOP
        WRITE(16) XHO
        WRITE(16) SAMINT
        WRITE(16) XPHAS
```

```
      WRITE(16) XTIME
      CLOSE(UNIT=16)
741   CONTINUE
      TYPE*,' '
      WRITE(15) NFILE
      write(15) (fr(i),i=1,NFILE)
      WRITE(15) ICON
      DO 333 M=1,NFILE
             FI(M)=0.
             FREQ=(2.*3.1415926535*FLOAT(M))/(FLOAT(NL)*SAMINT)
             FI(M)=FREQ/1000000.
333   CONTINUE
618   FORMAT(' ','FREQUENCY')
      WRITE(15) NFILE
      WRITE(15) (FI(I),I=1,NFILE)
      WRITE(15) XHO
      WRITE(15) SAMINT
      WRITE(15) XMAGN
      WRITE(15) XFREQ
      close(unit=15)
997   type*,'DO YOU WANT ANOTHER'
      TYPE*,'TRANSFORM? (1=YES,0=NO)'
      accept*,nragan
      if(nragan.ne.1)goto998
             goto01
998   continue
      stop
      end
```